Replenishing IRAK-M expression in retinal pigment epithelium attenuates outer retinal degeneration

Short title: Impaired IRAK-M in RPE promotes retinal degeneration

Jian Liu [1]*, David A. Copland [1], Alison J. Clare [1], Mathias Gorski [2], Burt T. Richards[3], Louis Scott[1], Sofia Theodoropoulou [1], Ursula Greferath [4], Katherine Cox [1], Gongyu Shi [1], Oliver H. Bell [1], Kepeng Ou [1], Jenna Le Brun Powell [5], Jiahui Wu [1], Luis Martinez Robles [6], Yingxin Li [5], Lindsay B. Nicholson[1,6], Peter J. Coffey [7], Erica L. Fletcher [4], Robyn Guymer [8], Monte J. Radeke [9], Iris M. Heid[2], Gregory S. Hageman[3], Ying Kai Chan [1,10], Andrew D. Dick [1,6,7,11]

[1]Academic Unit of Ophthalmology, Bristol Medical School, University of Bristol, Bristol BS8 1TD, UK.
[2]Department of Genetic Epidemiology, University of Regensburg, Regensburg 93053, Germany.
[3]Sharon Eccles Steele Center for Translational Medicine, John A. Moran Eye Center, University of Utah School of Medicine, Salt Lake City, UT 84132, USA.
[4]Department of Anatomy and Physiology, University of Melbourne, Melbourne, VIC 3010, Australia.
[5]Translational Health Sciences, Bristol Medical School, University of Bristol, Bristol BS8 1TD, UK.
[6]School of Cellular and Molecular Medicine, University of Bristol, Bristol BS8 1TD, UK.
[7]Institute of Ophthalmology, University College London, London EC1V 9EL, UK.
[8]Centre for Eye Research Australia, Royal Victorian Eye and Ear Hospital, University of Melbourne, Melbourne, VIC 3010, Australia.
[9]Neuroscience Research Institute, University of California, Santa Barbara, CA 93106, USA.
[10]Wyss Institute for Biologically Inspired Engineering, Harvard University, Boston, MA 02215, USA.
[11]National Institute for Health Research Biomedical Research Centre, Moorfields Eye Hospital, London EC1V 2PD, UK.

*Corresponding author. Email: jian.liu@bristol.ac.uk

Abstract

Chronic inflammation is a constitutive component of many age-related diseases, including age-related macular degeneration (AMD). Here, we identified interleukin-1 receptor–associated kinase M (IRAK-M) as a key immunoregulator in retinal pigment epithelium (RPE) that declines during the aging process. Rare genetic variants of *IRAK3*, which encodes IRAK-M, were associated with an increased likelihood of developing AMD. In human samples and mouse models, IRAK-M abundance in the RPE declined with advancing age or exposure to oxidative stress and was further reduced in AMD. *Irak3*-knockout mice exhibited an increased incidence of outer retinal degeneration at earlier ages, which was further exacerbated by oxidative stressors. The absence of IRAK-M led to a disruption in RPE cell homeostasis, characterized by compromised mitochondrial function, cellular senescence, and aberrant cytokine production. IRAK-M overexpression protected RPE cells against oxidative or immune stressors. Subretinal delivery of adeno-associated virus (AAV)–expressing human *IRAK3* rescued light-induced outer retinal degeneration in wild-type mice and attenuated age-related spontaneous retinal degeneration in *Irak3*-knockout mice. Our data show that replenishment of IRAK-M in the RPE may redress dysregulated pro-inflammatory processes in AMD, suggesting a potential treatment for retinal degeneration.

Teaser

IRAK-M protects the retinal pigment epithelium and is a potential therapeutic target for macular degeneration.

Editor's summary

Age-related macular degeneration (AMD) progression is associated with chronic inflammation, but the role of the Myddosome complex, which is necessary for Toll-like receptor and IL-1R signaling, in AMD has not been fully elucidated. Here, Liu and colleagues identified rare variants in *IRAK3*, which encodes the inhibitory Myddosome component IRAK-M, as being associated with an increased risk of late AMD. Using human retinal samples and mouse models of aging and retinal injury, as well as *Irak3*-knockout mice, the authors showed that IRAK-M was present in retinal pigment epithelium (RPE) and decreased with age and injury. Overexpression of human *IRAK3* in the RPE could attenuate outer retinal degeneration in these mouse models, suggesting a potential therapeutic strategy for AMD. —Melissa L. Norton

INTRODUCTION

Cell-autonomous responses, such as metabolic regulation, autophagy, and immune-mediated inflammation, initiated by environmental stressors are active processes that help to maintain homeostasis (*1*). However, loss of immune regulation and persistent inflammation can lead to acute or chronic tissue damage. Chronic inflammation, accentuated by aging (inflammaging), is implicated in the progression of many age-related degenerative disorders (*2*).

The retinal pigment epithelium (RPE) is essential for maintaining outer retinal function and ocular immune privilege. RPE dysfunction results in photoreceptor (PR) loss and gradual decline of the central visual acuity, as observed in age-related macular degeneration (AMD) (*3–5*). AMD, a progressive, multifactorial disease, is a leading cause of irreversible severe vision loss among the elderly. Alongside aging, the interplay of oxidative stress and chronic inflammation, fueled by genotype-predisposed susceptibility and environmental stressors, contributes substantially to the pathogenesis of AMD. Genome-wide association studies (GWAS) have identified risk loci for AMD, including genes in the complement pathway and *age-related maculopathy susceptibility 2* (*ARMS2*)/*HtrA serine peptidase 1* (*HTRA1*) alleles (*6, 7*). Rare coding variants in complement regulatory genes such as complement factor H (*CFH*) and complement factor I (*CFI*) have been associated with AMD risk, leading to the development of complement inhibitors and gene therapies (*8, 9*). AMD pathogenesis involves multiple pathways, including oxidative stress and innate immune responses (*10, 11*). In mice, for example, a high-fat diet is required to initiate pathology on the background of complement gene mutation (*12*). Therefore, elucidating the factors central to the diverse pathologies in AMD is critical, irrespective of genetic risk.

Several inflammatory pathways are associated with AMD progression, including the activation of the complement cascade, NLRP3 (nucleotide-binding domain, leucine-rich–containing family pyrin domain containing 3) inflammasome, production of cytokines and chemokines, immune cell infiltration, and immune activation of retinal microglia and RPE (*13–17*). Toll-like receptors (TLRs), particularly TLR2, -3, and -4, are implicated in AMD development (*18–20*). The Myddosome, an oligomeric complex consisting of myeloid differentiation primary response 88 (MyD88) and interleukin-1 (IL-1) receptor (IL-1R)–associated kinase (IRAK) family proteins, is essential for transmitting TLR and inflammasome–IL-1R axis–mediated signals (*16*). Myddosome signaling also promotes inflammasome activation (*21*). Although Myddosome overactivation has been observed in RPE from patients with geographic atrophy (late-stage atrophic AMD) (*16*), questions remain regarding its role in AMD progression and the specific Myddosome components driving TLR/IL-1R pro-inflammatory signaling dysregulation.

The RPE exhibits a high number of differentially expressed genes overlapping with those

associated with aging and age-related retinal diseases (*22*). Disturbances in RPE intracellular processes, such as autophagy and senescence, compounded by oxidative stress, lead to inflammasome activation and IL-1β/IL-18 release (*17*, *23*, *24*). The magnitude of oxidative stress–induced inflammation is largely determined by various TLRs and balanced by counteracting mechanisms regulated by inhibitors including IRAK-M (encoded by *IRAK3*) (*25*, *26*). IRAK-M is a pseudokinase that down-regulates the pro-inflammatory cascade by impeding phospho-IRAK1/4 uncoupling from the Myddosome for transforming growth factor–β (TGF-β)–activated kinase 1 (TAK1)–dependent nuclear factor–κB (NF-κB) activation, or by inducing downstream anti-inflammatory responses through the IRAK-M/MyD88 complex and IRAK-M/MEKK3 (mitogen-activated protein kinase kinase kinase 3) pathway (*27*, *28*).

IRAK-M expression is regulated by both epigenetic and transcriptional mechanisms, in response to numerous endogenous and exogenous factors including IL-1β, TGF-β1, granulocyte-macrophage colony-stimulating factor (GM-CSF), and adiponectin, as well as cell surface receptors or intracellular molecules including TLRs, triggering receptor expressed on myeloid cells 1 and phosphoinositide 3-kinase (*29*, *30*). Down-regulation of IRAK-M signaling is associated with exaggerated oxidative stress and systemic inflammation in metabolic disorders such as insulin resistance and obesity (*31*). Reduced *IRAK3* mRNA expression in monocytes and adipose tissues of obese patients leads to elevated mitochondrial stress, systemic inflammation, and metabolic syndrome (*31*). Multiple mutations in *IRAK3* have been associated with early-onset chronic asthma in humans (*32*).

Given *IRAK3* expression in RPE cells in vitro (*23*), we hypothesized its potential regulatory relevance in retinal aging and degeneration. The present study aimed to elucidate the role of IRAK-M in AMD by assessing genetic variants and their association with AMD risk. We also evaluated IRAK-M expression in patient samples and mouse models of retinal degeneration, alongside alterations in retinal function in *Irak3*-knockout (KO) mice. Furthermore, we explored the therapeutic potential of IRAK-M augmentation in protecting RPE and outer retina against degenerative processes in murine models.

RESULTS

Rare protein-altering variants of *IRAK3* are associated with an increased risk of late AMD

Given the observation of Myddosome activation in AMD (*16*), we asked whether variants in the

genes encoding Myddosome components contribute to disease risk and pathogenic pathways. Single variant analyses have limited power to depict rare variants with association. Gene-based burden tests, which assess accumulated association from multiple rare variants per gene, complement such analyses and enhance the ability to detect a disease burden. Hence, we applied burden tests of the genetic data from the International AMD Genomics Consortium (IAMDGC) which contains 16,144 late AMD cases versus 17,832 age-matched controls (*6*). The analysis revealed no association between rare variants of *MYD88* and late AMD ($P = 0.95$). We then examined the cumulative effect of rare protein-altering variants for the IRAK family kinases (*IRAK1–4*), which revealed a statistically significant late AMD risk–increasing signal for *IRAK3* ($P = 0.012$) (Table 1). Table S1 lists the variants in the *IRAK3* gene region, including 18 polymorphic variants that were detected in both AMD cases and controls and used in the gene burden test. As a comparator for *IRAK3*, rare variants of *IL33*, which encodes a T_H2 (T helper 2)-oriented cytokine linked to retinal pathophysiology (*33–35*), were not associated with late AMD ($P = 0.18$).

Table 1. Rare protein-altering variants of *IRAK3* are associated with increasing risk of late AMD.

The cumulative effect of rare protein-altering variants in the 16,144 late AMD cases versus 17,832 controls of four *IRAK* genes in the IAMDGC data was examined using gene burden test.

Gene symbol	CHROM	Start	End	*N* markers	Increasing/decreasing risk for AMD	*P* value
IRAK3	12	66,582,994	66,648,402	18	Increasing risk	0.012
IRAK1	X	153,278,500	153,284,192	2	Increasing risk	0.35
IRAK2	3	10,219,555	10,280,654	12	Increasing risk	0.91
IRAK4	12	44,172,041	44,177,510	3	Decreasing risk	0.22

IRAK-M expression in the RPE is reduced with age and to a greater extent in AMD

We next explored IRAK-M expression in the retina by performing immunohistochemistry (IHC) on human retinal cryosections from a young-age normal eye (age and gender details reported in table S2). We found abundant IRAK-M distribution at the RPE layer, with faint or subtle immunopositivity observed in other retinal layers, including GCL (ganglion cell layer), IPL (inner plexiform layer), OPL (outer plexiform layer), ONL (outer nuclear layer), POS (PR outer segment), and choroid (Fig. 1, A and B). IHC of a second donor eye also demonstrated IRAK-M expression in RPE and choroid in sections from an old-age normal eye (fig. S1, A and B, and table S2). IRAK-M was detected in mouse RPE (fig. S1, C to E), consistent with our previously reported detection of *Irak3* transcript in a murine RPE cell line (*23*). We observed strong immunopositivity of IRAK-M in both inner (nonpigmented) and outer (pigmented) ciliary epithelium of human eyes (fig. S1, F and G), suggesting a potential regulatory role in barrier cells.

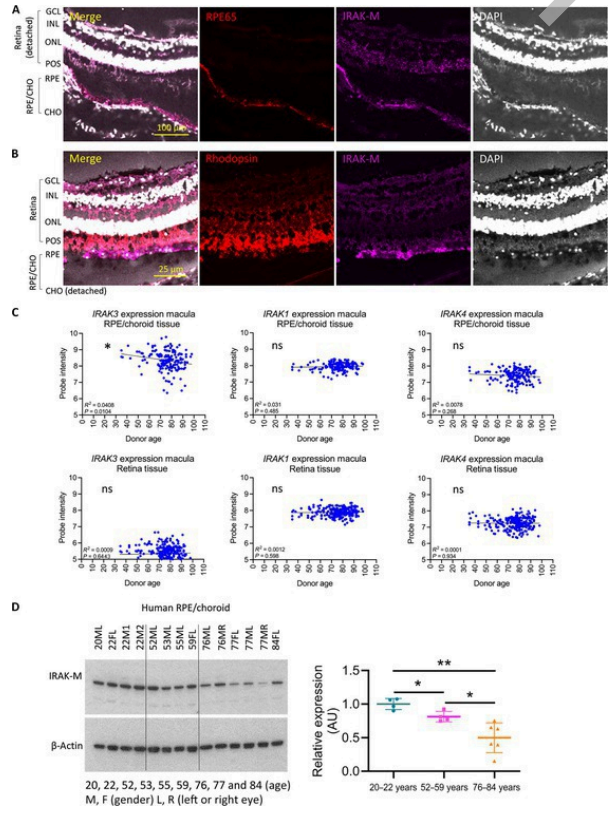

Fig. 1. IRAK-M is abundant in the RPE and its expression is reduced with age. (**A** and **B**) Confocal images of human retinal sections from a 20-year-old donor (without recorded ocular disease). Anti-RPE65 was used to stain the RPE [red, (A)], anti-rhodopsin was used to stain the photoreceptor outer segment [red, (B)], and 4′,6-diamidino-2-phenylindole (DAPI) was used to stain nuclei [white, (A and B)]. GCL, ganglion cell layer; INL, inner nuclear layer; ONL, outer nuclear layer; POS, photoreceptor outer segment; RPE, retinal pigment epithelium; CHO, choroid. (**C**) Graphs showing relative probe intensities for *IRAK3*, *IRAK1*, and *IRAK4* in the RPE/choroid (top) and retina (bottom), according to the age of the donor, as assessed by microarray. (**D**) Western blots (left) and densitometry quantification (right) of IRAK-M abundance in human RPE/choroidal lysates. Donor age, sex, and eye are indicated at the top of the blot. IRAK-M abundance was normalized to β-actin (20 to 22 years: $n = 4$; 52 to 59 years: $n = 4$; 76 to 84 years: $n = 6$). $^{*}P < 0.05$; $^{**}P < 0.01$; ns, nonsignificant. Comparison by simple linear regression (C), or one-way Brown-Forsythe and Welch ANOVA test with Dunnett's T3 tests (D).

We next determined whether the abundance of IRAK-M altered during aging. Total RNA was harvested from 6-mm trephine tissue punches of 227 extramacular and 159 macular RPE/choroids, as well as 238 extramacular and 242 macular retinas. Total RNA yield and RNA integrity number (RIN) scores were measured to confirm the consistency of the quality of RNA samples across the ages (fig. S2, A and B). Microarray analysis of these samples identified an age-dependent decrease in *IRAK3* expression in the macular ($R^2 = 0.0408$, $P = 0.0104$; Fig. 1C) and extramacular ($R^2 = 0.0403$, $P = 0.0025$; fig. S2C) RPE/choroid but no change in expression in the retina (Fig. 1C and fig. S2D). Neither *IRAK1* nor *IRAK4* expression changed with age in RPE/choroid or retina (Fig. 1C and fig. S2, C and D). Further analyses of IRAK-M protein abundance in sex-mixed human RPE/choroid lysates across a range of age groups (table S2) revealed significant reduction in samples from elderly individuals (76 to 84 years) compared to young (20 to 22 years, $P = 0.004$) or middle-aged (52 to 59 years, $P = 0.041$) samples (Fig. 1D). Increased abundances of phospho-IRAK4 and phospho–NF-κB p65 were also detected (fig. S3A), suggesting activation of inflammatory signaling pathways. CFH and C3 protein abundance did not change with age (fig. S3A). As with human samples, RPE isolated from aged mice (19 to 24 months) had lower IRAK-M protein abundance compared with younger mice (2 to 5 months; fig. S3B). The abundance of IRAK-M protein in mouse retinal $CD11b^{+}$ cells (magnetic-activated cell sorting–isolated microglia and perivascular macrophages) was also reduced with age (fig. S3C).

To ascertain whether *IRAK3* expression was compromised in AMD, as compared to age-matched controls, we analyzed a published RNA sequencing (RNA-seq) dataset (GSE99248), which included PORT-normalized counts for both sense and antisense transcripts (*36*). In the *IRAK* family genes, only *IRAK3* mRNA in RPE/choroid/sclera, and not in the retina, was lower in AMD than age-matched controls (Fig. 2A). *IRAK1*, *IRAK2*, and *IRAK4* expression, as well as antisense RNAs specific to any *IRAK*, were unchanged between AMD and controls (Fig. 2A). From the same dataset, we also examined the expression of other known genes for negative regulation of TLR/IL-1R/MyD88/IRAK1/4 signaling (fig. S4), including *PIN1* (peptidylprolyl cis/trans isomerase, NIMA-interacting 1, which inhibits TLR transcription factor IRF3), *IL1RN* (IL-1R antagonist), *SOCS1* (suppressor of cytokine signaling 1, which induces MAL ubiquitination required for MyD88 activation), *TOLLIP* (Toll-interacting protein, which binds to IRAK1 to induce translocation of TLRs to endosome for degradation), *FADD* (Fas-associated death domain, which interacts with IRAK1/MyD88 to attenuate the signaling), and *PTPN6* (tyrosine-protein phosphatase non-receptor type 6, which inhibits SYK activation and blocks MyD88 phosphorylation). None of these genes showed any significant difference between AMD and controls ($P > 0.05$; fig. S4).

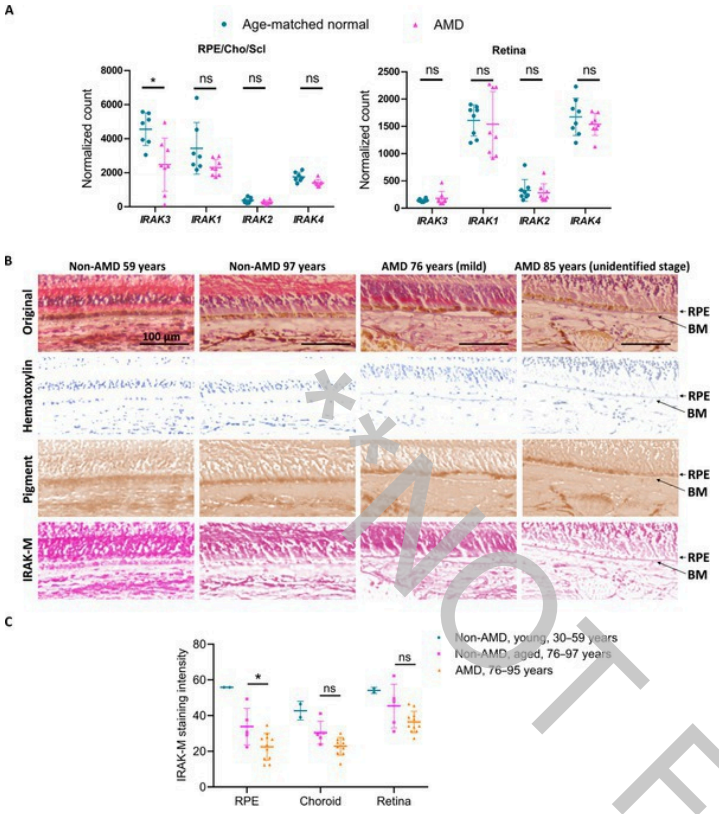

Fig. 2. IRAK-M expression in RPE is reduced in AMD.
(**A**) PORT-normalized gene counts from RNA-seq data (GSE99248) of *IRAK3*, *IRAK1*, *IRAK2*, and *IRAK4* in the RPE/choroid/sclera (left: $n = 8$ AMD, pink; $n = 7$ age-matched controls, teal) and retina (right: $n = 8$ AMD, pink; $n = 8$ controls, teal). (**B**) Representative IHC images (top row) of human retinal sections from two donors without AMD (non-AMD, 59 and 97 years old, respectively), a donor with mild AMD (76 years old), and a donor with AMD at unidentified stage (85 years old) were color-deconvoluted using ImageJ to separate IRAK-M staining (red, bottom row), pigment (brown, third row), and nuclei (blue, second row). Scale bars, 100 µm. Lower magnification images are shown in fig. S5. (**C**) Quantification of mean staining intensity of the RPE, choroid, and retina for IRAK-M abundance ($n = 2$ non-AMD young, teal; $n = 5$ non-AMD aged, pink; $n = 11$ AMD, orange). *$P < 0.05$. Comparison by multiple unpaired two-tailed Welch's *t* tests [RPE/Cho/Scl in (A)] or Mann-Whitney *U*-tests [retina in (A)] followed by Sidak-Bonferroni correction, or two-way ANOVA with Bonferroni post hoc tests (C).

To further determine the spatial expression of IRAK-M protein within tissue associated with

age and AMD, we performed IHC on paraffin-embedded retinal sections of 2 "young" (30 and 59 years old) and 5 "aged" (76 to 97 years old) individuals without recorded ocular diseases and 11 patients with AMD (76 to 95 years old). Table S2 contains detailed age and sex information for these samples. The paraffin slides were visualized using alkaline phosphatase-based IHC due to the strong autofluorescence of the RPE that was not fully blocked by Sudan black B quenching. IRAK-M (stained in red) was observed in multiple layers of the retina, RPE, and choroid (non-AMD 59 years; Fig. 2B and fig. S5A). In aged control and AMD samples, the pattern and strength of IRAK-M–immunopositive signals was variable, for example, with a heightened signal in OPL/ONL (non-AMD 97 years; Fig. 2B and fig. S5B), INL/ONL/IS (inner segment) (mild AMD 76 years; Fig. 2B and fig. S5C), or NFL (nerve fiber layer) (unidentified stage AMD 85 years; Fig. 2B and fig. S5D). Furthermore, we observed an intensified Bruch's membrane in retinal sections of patients with AMD (Fig. 2B), which was not seen in non-AMD samples (*37*). After color deconvolution using the Fiji package of ImageJ, IRAK-M signal (red) and RPE pigment (brown) were separated for quantification. IRAK-M expression was lower in AMD-macular RPE compared to age-matched non-AMD–macular RPE (Fig. 2C). In macular areas of choroid or retina, despite a trend of reduction in AMD, the difference in IRAK-M expression between AMD and age-matched non-AMD was not statistically significant ($P > 0.05$; Fig. 2C). In extramacular tissues, IRAK-M expression in RPE, choroid, or retina did not significantly differ between AMD and non-AMD samples ($P > 0.05$; fig. S6).

Irak3-KO mice acquire earlier outer retinal degeneration during aging

We then investigated whether aging and lack of *Irak3* affected outer retinal degeneration in *Irak3*-KO mice (*Rd8* mutation removed, as confirmed in fig. S7A). In this strain, the exons 9 to 11 of *Irak3* were removed by homologous recombination, resulting in a mutant IRAK-M protein missing two-thirds of the pseudokinase domain (*38*, *39*). The multiple conserved cysteine residues within the dimeric structure of the pseudokinase domain of native IRAK-M are essential in forming an interactive interface with IRAK4 for the negative regulation of IRAK-Myddosome signaling (*40*).

Pathological changes in the retina were tracked for 15 months using fundoscopy and optical coherence tomography (OCT). Repeated imaging of the same affected retinas unveiled the emergence of white spots with aging (Fig. 3A), along with an increase in the number of retinas displaying varying counts of fundus white spots in *Irak3*-KO mice, elevating from 5 out of 22 eyes

at 2 months to 15 out of 30 eyes at 5 months (Fig. 3, A and B, and fig. S7B). Fundus white spots in mice have been well described as a feature of foci of inflammation linked to accumulated macrophages/microglia in the outer retina and subretinal space, where they phagocytose-damaged PRs and RPE (*41–45*). The incidence of abnormal retinal appearance reached 21 out of 26 by 15 months (Fig. 3B). In comparison, there was no progression of white spots in the retinas of wild-type (WT) mice to 12 months; however, WT retinas displaying white spots markedly increased as mice aged, with16 out of 26 retinas displaying white spots by 19 to 21 months (Fig. 3B). These data suggest accelerated aging-associated retinal abnormalities and degeneration associated with *Irak3* mutation. We also noted that the early appearance of retinal white spots in *Irak3*-KO mice was accompanied by outer retinal lesions identified by OCT (Fig. 3C).

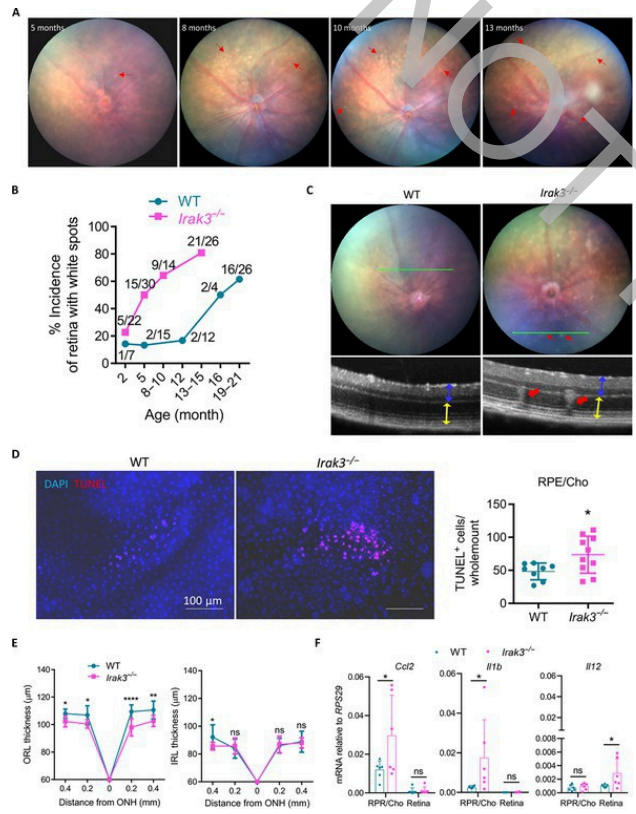

Fig. 3. *Irak3*$^{-/-}$ mice spontaneously display early retinal abnormalities.
(**A**) Representative fundal images of *Irak3*$^{-/-}$ mouse retinas at 5, 8, 10, and 13 months. White spots are indicated by red arrows. (**B**) Graph showing the incidence of the flecked retina (number of spots >3) in *Irak3*$^{-/-}$ mice (pink) compared to WT controls (teal) at

different ages. Each value is a ratio of the number of flecked retinas to the total number of retinas at each time point. (**C**) Representative fundal (top) and OCT (bottom) images from 5-month-old *Irak3*$^{-/-}$ mice. White spots are indicated by red arrows. Yellow double-arrow lines indicate the boundaries of outer retinal layers (ORL), and blue double-arrow lines indicate the boundaries of inner retinal layers (IRL). (**D**) TUNEL staining (left) and quantification (right) of RPE/choroidal flatmounts from *Irak3*$^{-/-}$ mice (pink, $n = 10$) versus WT controls (teal, $n = 8$) at 5 months of age. (**E**) Quantification of OCT images to assess ORL (left) and IRL (right) thickness in *Irak3*$^{-/-}$ mice (pink, $n = 11$) and WT controls (teal, $n = 12$) aged 12 to 13 months. (**F**) qRT-PCR analysis of mRNA expression of *Ccl2*, *Il1b*, and *Il12* (normalized to *RPS29*) in RPE/choroid tissues from 12-month-old *Irak3*$^{-/-}$ mice (pink, $n = 6$) and WT controls (teal, $n = 6$). *$P < 0.05$; **$P < 0.01$; ****$P < 0.0001$. Comparison by unpaired two-tailed Welch's *t* test (D) and two-way ANOVA followed by Bonferroni tests (E and F).

Given the link between fundus spots and microglia/macrophage activation in various murine models of retinal degeneration (*41–45*), we evaluated the CD11b^{+} myeloid cell populations in the murine retina. As expected, increased numbers of CD11b^{+} cells in the ONL (fig. S7C) and CD11b^{+} cell accumulation in the subretinal space (fig. S7D) were observed in *Irak3*$^{-/-}$ mice, associated with increased number of terminal deoxynucleotidyl transferase–mediated deoxyuridine triphosphate nick end labeling (TUNEL)–positive RPE cells in multiple focal areas on the surface of RPE/choroidal flatmounts (Fig. 3D). Although no difference in retinal thickness was found at 5 months between WT and *Irak3*$^{-/-}$ mice, the outer retina layers (ORL; see Supplementary Methods for definition) of *Irak3*$^{-/-}$ mice were thinner by 12 to13 months (Fig. 3E). By 12 months, there were significant increases ($P < 0.05$) in *Ccl2* (*chemokine C-C motif ligand 2*) and *Il1b* mRNA expression (normalized to *RPS29*) in *Irak3*$^{-/-}$ RPE/choroid compared to WT counterparts (Fig. 3F), suggesting a pro-inflammatory tissue environment. The relative mRNA expression of cytokines in the retina were all below 0.005 regardless of genotypes—much lower than those in RPE/choroid—although *Il12* expression was up-regulated in *Irak3*$^{-/-}$ retina (Fig. 3F). We were unable to compare tissue cytokine protein concentrations due to undetectability or trace amounts of the cytokines in RPE/choroid and retina samples. Systemically, concentrations of serum cytokines, including tumor necrosis factor–α (TNF-α), monocyte chemoattractant protein 1, and IL-10, in *Irak3*$^{-/-}$ mice were significantly higher than those in WT mice ($P < 0.05$; fig. S7E).

Oxidative stress reduces RPE IRAK-M abundance, and loss of IRAK-M increases the susceptibility of outer retinal layers to oxidative damage

Age-associated accumulation of oxidative stress in the RPE is a recognized contributor to the progression of AMD. To examine whether oxidative stress could be an independent factor for the reduction of IRAK-M, we applied oxidative stressors both in vitro and in vivo.

In vitro, we examined early passage (<8) human retinal pigment epithelial ARPE-19 cells to reduce variability. Confluent ARPE-19 cells exhibited RPE features, including cobblestone-like morphology, and expressed tight junction protein zonula occludens-1 (ZO-1) and RPE-specific protein RPE65 (fig. S8A). ARPE-19 cells were treated with different doses of paraquat for up to 72 hours to induce mitochondrial ROS, which caused dose-dependent cytotoxicity as assessed by a lactate dehydrogenase (LDH) cytotoxicity assay (fig. S8B). IRAK-M abundance was suppressed by 72-hour exposure to a sub-toxic dose of paraquat (0.25 mM) (fig. S8C). Reduction in IRAK-M was accompanied by increased secretion of pro-inflammatory cytokines HMGB1 (high mobility group box 1), IL-18, and GM-CSF and by decreased secretion of anti-inflammatory IL-11 (fig. S8D). Crucially, down-regulation of IRAK-M also occurred in human induced pluripotent stem cell (iPSC)–derived RPE cells after 72-hour treatment of sub-toxic doses of paraquat (0.25 to 0.5 mM) (fig. S8, E and F).

In vivo, retinal oxidative damage was introduced by fundus camera–directed light exposure (100 kilolux for 20 min) (*46*) or intravitreal administration of paraquat (2 μl at 1.5 mM) (*47*) in C57BL/6J WT mice at 8 weeks of age. Western blot analyses showed that IRAK-M abundance in the RPE lysate was abated after 7 days in both models (Fig. 4, A and B). In separate experiments, fundoscopy and OCT images obtained on day 14 displayed the fundal appearance of white spots (red arrows; Fig. 4, C and D), alongside thinning of the outer retina in the light-induced retinal degeneration (LIRD) model (Fig. 4E), as well as reduced thickness in outer and a partial decrease in inner retinal thickness in the paraquat model (Fig. 4F). Retinal oxidative stress was then induced in adult WT and *Irak3*$^{-/-}$ mice (8 weeks old) by light induction. *Irak3*$^{-/-}$ mice exhibited greater thinning of the retina after light challenge, particularly the ORL (Fig. 4G).

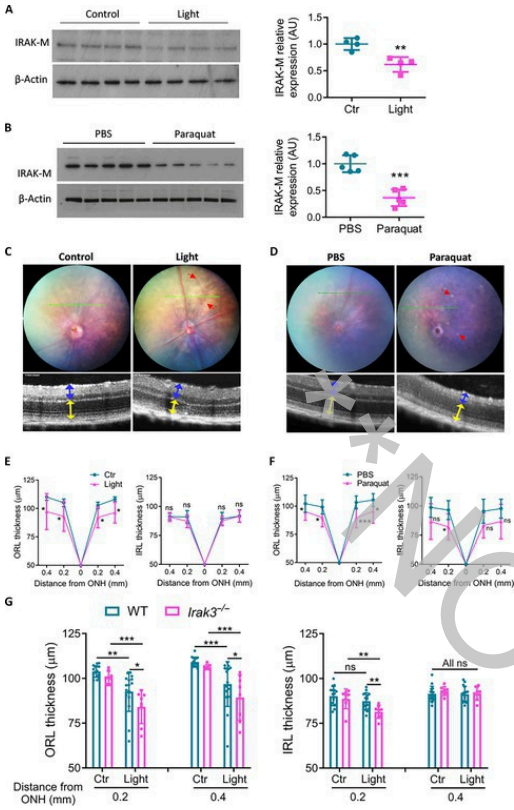

Fig. 4. Oxidative stress reduces IRAK-M abundance in the RPE of WT mice, and *Irak3*$^{-/-}$ mice are more vulnerable to light-induced retinal degeneration.

Retinal oxidative stress was induced in 8-week-old C57BL/6J mice by either fundus-light induction [100 kilolux for 20 min, (**A**, **C**, and **E**)] or intravitreal administration of paraquat [2 μl at 1.5 mM, (**B**, **D**, and **F**)]. (A) Western blots (left) and densitometry (right) showing IRAK-M abundance in RPE lysate on day 7 after light exposure (pink) compared with control (teal) (n = 4). (B) Western blots (left) and densitometry (right) showing IRAK-M abundance in RPE lysate on day 7 after paraquat injection (pink) compared with PBS control (teal) (n = 5). (C) Representative fundoscopy (top) and OCT images (bottom) obtained on day 14 after light exposure. (D) Fundoscopy (top) and OCT images (bottom) obtained on day 14 after the paraquat injection. Retinal lesions are indicated by red arrows, yellow double-arrow lines indicate the thickness of ORL, and blue double-arrow lines indicate the thickness of IRL. (E) Quantification of OCT images to assess ORL (left) and IRL (right) thickness in LIRD mice (pink, n = 8) and controls (teal, n = 8). (F) ORL (left) and IRL (right) thickness in paraquat-injected mice (pink, n = 11) and PBS-injected control (teal, n = 9). (**G**) Eight-week-old WT

and *Irak3*$^{-/-}$ mice were subjected to retina light-induced oxidative insults. Quantification of ORL (left) and IRL (right) thickness *Irak3*$^{-/-}$ mice (pink, $n = 8$) compared to WT controls (teal, $n = 16$) 14 days after light induction, as assessed by averaging of temporal and nasal measurements by OCT. *$P < 0.05$; **$P < 0.01$; ***$P < 0.001$. Comparison by unpaired two-tailed Student's *t*-test (A and B), or two-way ANOVA with Holm-Sidak post hoc tests (E, F, and G).

AP-1 regulates IRAK-M expression in RPE cells in an age-dependent manner

Known transcription factors regulating IRAK-M expression in monocytes or lung epithelial cells include AP-1 and C/EBP-β (*29*, *48*). We found that, in addition to an age-associated reduction in IRAK-M abundance (Fig. 1D), an abundance of c-Jun, an AP-1 subunit, was decreased in aged samples compared to young controls (fig. S9, A and B). c-Fos, another AP-1 subunit, was also reduced in old age compared to middle-aged samples, whereas there was no change in C/EBP-β abundance between samples (fig. S9, A and B).

The binding of c-Jun and c-Fos to the IRAK-M promoter region was confirmed by chromatin immunoprecipitation assay on ARPE-19 cells, and this was increased by lipopolysaccharide (LPS) stimulation for 24 hours (fig. S9C). ARPE-19 cells treated with paraquat for 72 hours showed decreased phosphorylation of both c-Jun and c-Fos, and total c-Jun and c-Fos were down-regulated by a higher dose of paraquat only (fig. S9D). The c-Jun N-terminal kinase inhibitor SP600125 or the c-Fos/AP-1 inhibitor T5224 at 20 μM also decreased IRAK-M abundance in ARPE-19 cells (fig. S9D). Consequently, treatment with SP600125 or T5224 resulted in enhanced ARPE-19 susceptibility to paraquat-induced cytotoxicity (fig. S9E), as did *IRAK3* siRNA (fig. S9F).

IRAK-M deficiency induces RPE mitochondrial dysfunction and senescent phenotype which is protected by IRAK-M augmentation

To elucidate metabolic mechanisms involved in IRAK-M deficiency–induced retinal degeneration, we examined RPE cell metabolism and senescence using primary mouse RPE cells. The RPE cells from *Irak3*$^{-/-}$ mice showed reduced basal mitochondrial respiration and adenosine triphosphate

production compared to WT (fig. S10A), whereas no differences in basal glycolysis and maximal glycolytic capacity were observed between genotypes (fig. S10B). These data suggest a role for IRAK-M in the maintenance of mitochondrial function in RPE cells. *Irak3*$^{-/-}$ RPE cells were more prone to oxidative stressor–induced (paraquat or H_2O_2) senescent phenotype, with increased activity of senescence-associated β-galactosidase (SA–β-Gal; fig. S10C), increased abundance of cyclin-dependent kinase inhibitor p21^{CIP1} and decreased nuclear lamin B1 (LB1; fig. S10D), and increased secretion of IL-6 (a senescence-associated cytokine) (fig. S10E) (*17*). The basal secretion of the pro-inflammatory cytokine HMGB1 of *Irak3*$^{-/-}$ RPE cells was higher than the WT cells, whereas secretion in response to oxidative stressors was comparable (fig. S10F).

We then examined whether overexpression of endogenous IRAK-M protein could protect RPE via CRISPR-Cas9–mediated gene expression. After the augmentation of IRAK-M abundance in human iPSC-derived RPE cells confirmed by Western blot (fig. S11A), the cells were treated with either H_2O_2 or LPS. Oxygen consumption rate analysis demonstrated that basal and maximal mitochondrial respiration were both sustained by IRAK-M overexpression but impaired in sham-transfected cells after oxidative or immune stresses (Fig. 5A). Although untreated IRAK-M–overexpressing iPSC-RPE cells displayed lower maximal glycolytic activity than control plasmid-transfected cells, glycolytic activity remained stable upon H_2O_2 or LPS treatment, whereas glycolytic activity in control cells was reduced by 24-hour treatment with H_2O_2 or LPS (Fig. 5B). The lower glycolytic activity in un-stressed iPSC-RPE with overexpressed IRAK-M may indicate lower bio-energetic dependency on glucose, suggesting possible benefits to glucose-dependent PRs (*49*).

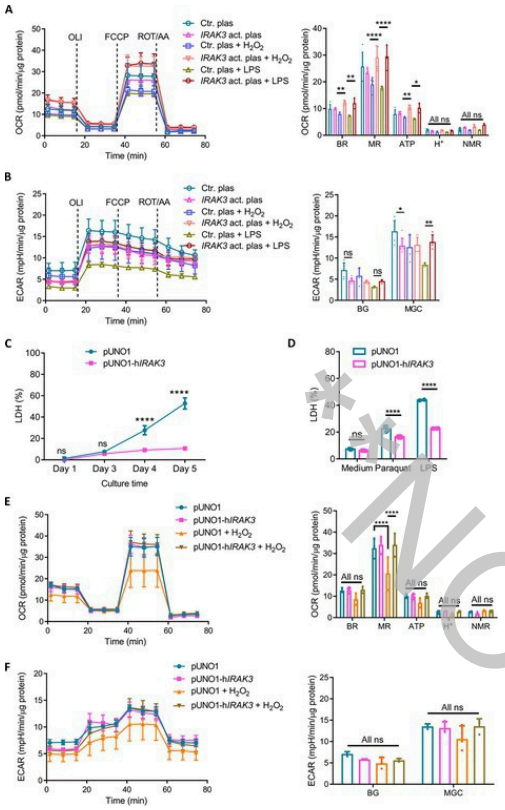

Fig. 5. Overexpression of *IRAK3* in RPE cells supports metabolic activities and inhibits cell death against stressors.

(**A** and **B**) Metabolic flux analysis of human iPSC-RPE cells transfected with *IRAK3* CRISPR activation plasmid or control plasmid for 48 hours, and then challenged by 30 μM H_2O_2 or LPS (1 μg/ml) for 24 hours. Oxygen consumption rate (OCR) (A) and ECAR (B) profile (left) and parameters (right) of the iPSC-RPE cells (n = 5 control plasmid group, teal; n = 6 *IRAK3* activation plasmid, pink; n = 4 control plasmid + H_2O_2, blue; n = 7 *IRAK3* activation plasmid + H_2O_2, orange; n = 3 control plasmid + LPS, lime; n = 4 *IRAK3* activation plasmid + LPS, maroon). (**C**) LDH cytotoxicity analysis of mouse B6-RPE07 cells stably transfected with pUNO1-human *IRAK3* plasmid (pink) or pUNO1 control plasmid (teal) over 5 days since confluency (day 1, day 4, day 5: n = 4; day 3: n = 8). (**D**) Cytotoxicity assay of stably transfected B6-RPE07 cells treated with paraquat (125 μM, n = 4) or LPS (40 ng/ml, n = 2) for 72 hours, compared to untreated cells (n = 4). (**E** and **F**) Metabolic flux analysis of transfected primary mouse *Irak3*$^{-/-}$ RPE cells treated by 60 μM H_2O_2 for 24 hours. OCR (E) and ECAR (F) profile (left) and parameters (right) of the cells (pUNO1, teal;

pUNO1-h*IRAK3*, pink; pUNO1 + H_2O_2, orange; pUNO1-h*IRAK3* + H_2O_2, brown; all $n = 3$). $^*P < 0.05$; $^{**}P < 0.01$; $^{****}P < 0.0001$. Comparison by two-way ANOVA with Bonferroni post hoc tests.

Overexpression of IRAK-M in ARPE-19 cells promoted the formation of autophagosomes [light chain 3B (LC3B)–green fluorescent protein (GFP)] and autolysosomes [LC3B–red fluorescent protein] after H_2O_2 or LPS treatment, suggesting an up-regulated autophagy flux (fig. S11, B and C). Moreover, IRAK-M overexpression in ARPE-19 cells ameliorated the SA–β-Gal activity and HMGB1 secretion induced by sub-toxic doses of paraquat (0.25 mM) (fig. S11, D and E) and reduced the LDH release induced by a toxic dose of paraquat (1 mM) (fig. S11F).

We created stably transfected RPE cell lines maintained in a selective medium from a parent mouse B6-RPE07 cell line that expressed either mouse *Irak3* or human *IRAK3* mRNA, as evidenced by quantitative reverse transcription polymerase chain reaction (qRT-PCR) (fig. S12A). Expression of mouse *Irak1* and *Irak4* was not affected. Human *IRAK3*-expressing mouse cells showed a decrease in DNA binding activity of NF-κB after LPS stimulation (fig. S12B), supporting the idea that transduced human *IRAK3* is as functional as its murine counterpart in suppressing NF-κB activation in mouse RPE. Stably transfected RPE cells overexpressing human *IRAK3* experienced less cytotoxicity than sham-transfected cells after 4 days of confluency (Fig. 5C) and exhibited reduced stressor-induced cytotoxicity after treatment with paraquat (0.125 mM) or LPS (40 ng/ml) for 3 days (Fig. 5D). To exclude the possible contribution of native mouse *Irak3* to cell response observed, we performed transient transfection on primary RPE cells isolated from *Irak3*$^{-/-}$ mice. Similar to data from human iPSC-RPE cells using CRISPR-Cas9 activation plasmid (Fig. 5, A and B), maximal mitochondrial respiration was retained in mouse primary *Irak3*$^{-/-}$ RPE cells transduced with human *IRAK3* after 24 h H_2O_2 treatment (Fig. 5E). H_2O_2-induced oxidative stress did not affect glycolysis in *Irak3*$^{-/-}$ RPE cells, regardless of human *IRAK3* transduction (Fig. 5F).

AAV2.cytomegalovirus promoter–mediated human *IRAK3* expression suppresses light-induced retinal degeneration in wild-type mice

To date, adeno-associated virus 2 (AAV2) is the best clinically validated AAV serotype to treat

RPE-related retinal pathologies when administrated subretinally and leads to durable gene expression and efficacy without inducing deleterious immune activation (*50*). In nonhuman primates and mice, subretinal injection of AAV2.cytomegalovirus (CMV) preferably transduces the RPE and, at higher doses, PRs (*51*, *52*).

We therefore administered AAV2.CMV subretinally to introduce human *IRAK3* expression in C57BL/6J mice. To identify the dose-dependent transduction efficacy, 2 μl of AAV2-encoding enhanced GFP (EGFP) under the control of the constitutive CMV promoter (AAV2.CMV.EGFP) at 1×10^{12} or 2×10^{11} genome copies (gc)/ml were subretinally delivered into mouse eyes. The "high dose" (1×10^{12} gc/ml in 2 μl or 2×10^{9} gc per eye) induced more pronounced EGFP expression 2 to 11 weeks after injection than the "low dose" (2×10^{11} gc/ml or 4×10^{8} gc per eye) (fig. S13). Administration with AAV2.CMV.h*IRAK3* induced a dose-dependent human *IRAK3* mRNA expression in RPE/choroid 2 weeks after injection, compared to a similar vector but with no transgene used as a control "null" vector (Fig. 6A). Low mRNA expression of exogenous human *IRAK3* was detected in the retina, at levels 17.1-fold lower than that in the RPE/choroid (Fig. 6A). Using an antibody specific to human IRAK-M protein, we confirmed that the exogenous IRAK-M was largely expressed in the RPE by IHC (Fig. 6B).

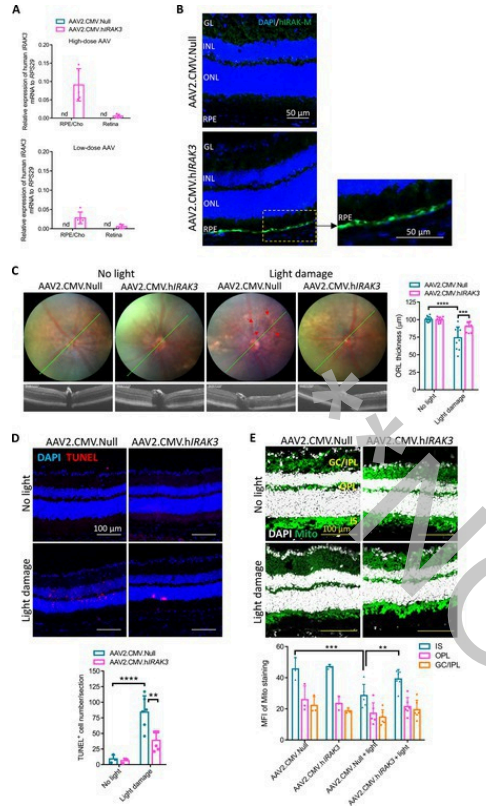

Fig. 6. Subretinal delivery of AAV2.CMV.h*IRAK3* protects against light-induced retinal damage in wild-type mice.

(**A**) Two weeks after subretinal injection of AAV2.CMV.h*IRAK3* or AAV2.CMV.Null (high dose 2×10^9 gc per eye, top; low dose 4×10^8 gc per eye, bottom), RPE/choroid and retina were analyzed for human *IRAK3* expression using qRT-PCR, normalized to *RPS29* ($n = 5$). (**B**) Retinal cryosections were examined for high-dose AAV-mediated IRAK-M expression using an antibody specific to human IRAK-M (green). DAPI staining of nuclei in blue. Representative confocal images were shown. (**C** to **E**) Two weeks after subretinal injection with the high dose of AAV2.CMV.h*IRAK3* or AAV2.CMV.Null, each mouse was subjected to light-induced retinal degeneration in one eye, followed by assessment of retinal pathology and therapeutic response after a further 2 weeks. (C) Representative fundoscopy (top left), OCT images (bottom left), and quantification (right) show light-induced retinal lesions (red arrows) and averaged ORL thickness in AAV2.CMV.h*IRAK3*-treated ($n = 10$, pink) or AAV2.CMV.Null-treated ($n = 11$, teal) mice. (D) Representative confocal images of TUNEL staining on retinal sections (top) and quantification (bottom) of three sections from each eye

treated with AAV2.CMV.h*IRAK3* (pink) or AAV2.CMV.Null (teal). $n = 6$ for light challenge groups; $n = 3$ for control (no light challenge) groups. (E) Confocal images of MitoView Green staining for mitochondrial content (top: DAPI staining shown in white) and mean fluorescence intensity (MFI) measurement (bottom) in three different fields from two sections of each eye treated with AAV2.CMV.h*IRAK3* or AAV2.CMV.Null. MFI analysis was performed at different retinal layers (IS: inner segment, teal; OPL: outer plexiform layer, pink; GC/IPL: ganglion cell/inner plexiform layer, orange). $n = 6$ for light damage groups; $n = 3$ for no light groups. $^{**}P < 0.01$; $^{***}P < 0.001$; $^{****}P < 0.0001$. Comparison by two-way ANOVA followed by Bonferroni tests (C to E).

To evaluate the protective effects of *IRAK3* transgene expression in vivo, we applied LIRD in mice 2 weeks after AAV injection (2×10^9 gc per eye). Light exposure of the null AAV2-injected eyes resulted in a decrease of outer retinal thickness, whereas AAV2.CMV.h*IRAK3* treatment reduced light-induced outer retinal thinning 2 weeks after light exposure (Fig. 6C). TUNEL staining in the ONL was also reduced by AAV2.CMV.h*IRAK3* (Fig. 6D). Mitochondrial staining in the IS was improved in LIRD mice treated with AAV2.CMV.h*IRAK3* compared to null AAV2-injected mice (Fig. 6E). The differences of mitochondrial staining in the GCL, IPL, and OPL between control and LIRD mice were not significant ($P > 0.05$), irrespective of AAV2.CMV.h*IRAK3* treatment (Fig. 6E).

RPE-specific *IRAK3* expression attenuates light-induced RPE and outer retinal degeneration in wild-type mice

We next used the RPE-specific bestrophin-1 (Best1) promoter to elucidate whether AAV2-mediated overexpression of *IRAK3* exclusively in the RPE also conferred protection. In line with previous data showing the superiority of CMV promoter over Best1 promoter in driving transgene expression in mouse RPE (*53*, *54*), we found that AAV2.Best1 required a higher multiplicity of infection (MOI 100,000) to ensure comparable expression of human *IRAK3* mRNA in mouse B6-RPE07 cells than AAV2.CMV (MOI 50,000) (fig. S14). Similarly, a two times higher AAV2.Best1 vector dose (4×10^9 gc per eye) than AAV2.CMV (2×10^9 gc per eye) was needed to give a robust expression of human IRAK-M protein in the RPE of mice (Fig. 7A). We, therefore, used AAV2.Best1.h*IRAK3* at 4×10^9 gc per eye and AAV2.CMV.h*IRAK3* at 2×10^9 gc per eye for subsequent treatments.

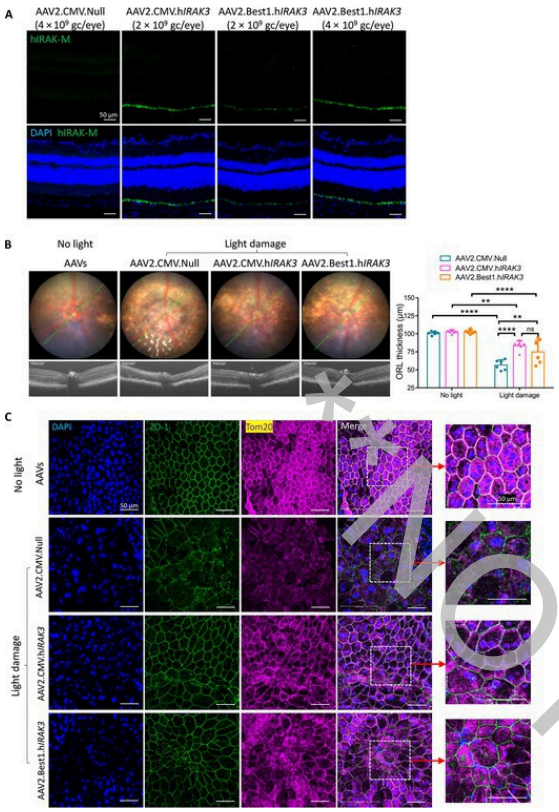

Fig. 7. Higher dose of AAV2.Best1.h*IRAK3* is required to transduce comparable expression of exogenous IRAK-M as AAV2.CMV.h*IRAK3*.

(**A**) Two weeks after subretinal injection of AAV2.CMV.h*IRAK3* (2×10^9 gc per eye), AAV2.Best1.h*IRAK3* (2 or 4×10^9 gc per eye), or AAV2.CMV.Null (2 or 4×10^9 gc per eye), retinal cryosections were prepared and stained with an antibody specific to human IRAK-M. Representative confocal images show the staining of transduced human IRAK-M (green) and DAPI (blue). (**B** and **C**) Three weeks after subretinal delivery of AAV2.CMV.h*IRAK3* (2×10^9 gc per eye), AAV2.Best1.h*IRAK3* (4×10^9 gc per eye), or AAV2.CMV.Null (2 or 4×10^9 gc per eye), each mouse was subjected to a fluorescein (FL)-assisted light-induced retinal degeneration in one eye and assessment of retinal pathology and therapeutic response were undertaken two weeks later. (B) Representative fundoscopy (top left), OCT images (bottom left), and quantification (right) of averaged ORL thickness ($n = 6$ to 7). (C) Representative confocal images of RPE flatmounts stained for tight junction protein ZO-1 (green) and mitochondrial marker Tom20 (magenta). DAPI is shown in blue. Higher magnification panels on right. $^{**}P < 0.01$; $^{****}P < 0.0001$. Comparison by two-way

ANOVA followed by Bonferroni tests (B).

To evaluate the therapeutic effects of *IRAK3* gene therapy under a more severe experimental setting, we augmented outer retinal damage using a fluorescein (FL)-assisted LIRD model that renders the retina more susceptible to light exposure (*46*, *55*). Three weeks after subretinal delivery of AAV2.CMV.h*IRAK3* (2×10^9 gc per eye), AAV2.Best1.h*IRAK3* (4×10^9 gc per eye), or AAV2.CMV.Null (2×10^9 or 4×10^9 gc per eye), WT mice were subjected to the FL-assisted light injury (*46*). Two weeks after light exposure, whereas the FL-assisted approach in null vector-injected control eyes caused a reduction in ORL thickness by 43.9%, both AAV2.CMV.h*IRAK3* and AAV2.Best1.h*IRAK3* reduced the degree of ORL thinning (Fig. 7B). Whole RPE flatmounts were stained with antibodies recognizing a tight junction-associated protein (ZO-1) and a mitochondrial marker (translocase of outer mitochondrial membrane 20, Tom20). Three representative areas 0.4 mm distant from the optic nerve head of each flatmount were imaged. Light exposure induced RPE disorganization and mitochondrial damage, demonstrated by the appearance of enlarged cells, disarray of hexagonal morphology, and loss of staining for ZO-1 and Tom20 (Fig. 7C). AAV2.CMV.h*IRAK3* and AAV2.Best1.h*IRAK3*, each resulted in amelioration of RPE morphological abnormalities and preservation of ZO-1 and Tom20 staining. Tom20 staining was more pronounced adjacent to the cell membrane of RPE cells (Fig. 7C), suggesting mitochondrial mobilization toward the intercellular junction sites (*56*).

AAV2.CMV-mediated *IRAK3* expression suppresses spontaneous outer retinal degeneration in *Irak3*$^{-/-}$ mice

We then investigated whether AAV-*IRAK3* could attenuate outer retinal degeneration caused by *Irak3*-KO and aging. We administered AAV2.CMV.h*IRAK3* or AAV2.CMV.Null (2×10^9 gc per eye) subretinally in young *Irak3*$^{-/-}$ mice (2 to 4 months old) and allowed them to age. Six months after subretinal delivery of AAV vectors, AAV2.CMV.h*IRAK3* blunted the age-dependent occurrence of retinal spots (Fig. 8, A and B) and reduced the number of retinal spots in *Irak3*$^{-/-}$ mice compared to AAV2.CMV.Null (8 to 10 months old; Fig. 8C). The effect was more pronounced within the treatment side of the retina receiving the vector, as expected (Fig. 8C). Compared to AAV2.CMV.Null-treated mice, mice receiving AAV2.CMV.h*IRAK3* experienced less outer retinal thinning at 0.2 mm from the optic nerve head (Fig. 8D).

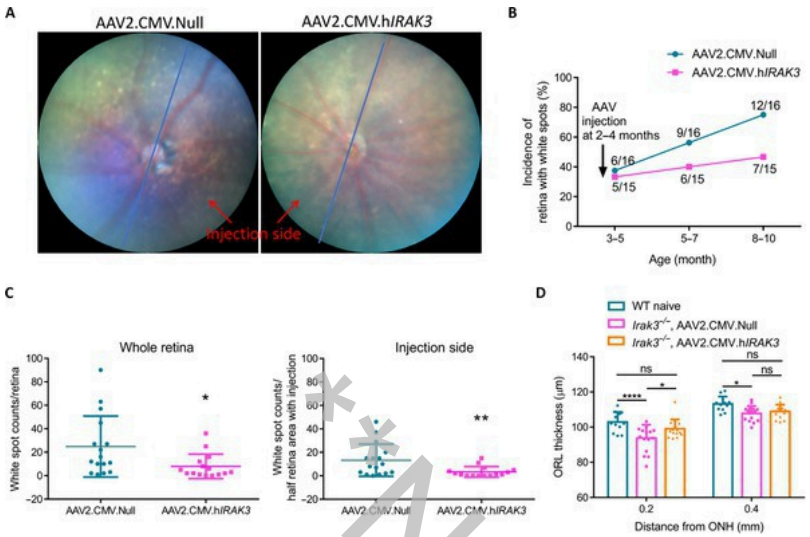

Fig. 8. Subretinal delivery of AAV2.CMV.h*IRAK3* prevents age-related spontaneous retinal degeneration in *Irak3*$^{-/-}$ mice.

A total of 2 × 10^9 gc of AAV2.CMV.h*IRAK3* were injected subretinally in one eye of each *Irak3*$^{-/-}$ mouse (2 to 4 months old), with AAV2.CMV.Null injected subretinally into the contralateral eye. Mice were then monitored by fundoscopy and OCT for 6 months. (**A**) Representative fundal images of 8-month-old *Irak3*$^{-/-}$ mice with AAV administration at the age of 2 months. Blue lines separate the retina into two sides based on the injection site (indicated by red arrows). (**B**) Time course of incidence of flecked retina in *Irak3*$^{-/-}$ mice treated with AAV2.CMV.h*IRAK3* (n = 15, pink) or AAV2.CMV.Null (n = 16, teal). (**C**) Numbers of retinal spots in the whole retina (left) or on the injection side (right) were blind-counted for comparison between AAV2.CMV.h*IRAK3* (n = 15, pink) and AAV2.CMV.Null-treated (n = 16, teal) mice at 8 to 10 months of age. (**D**) OCT quantification of ORL thickness at 0.2 and 0.4 mm distant from the optic nerve head in 8- to 10-month-old *Irak3*$^{-/-}$ mice treated with AAV2.CMV.h*IRAK3* (n = 15, orange), 8- to 10-month-old *Irak3*$^{-/-}$ mice treated with AAV2.CMV.Null (n = 16, pink), and WT littermates (n = 12, teal) that did not receive injections. *P < 0.05; **P < 0.01; ****P < 0.0001. Comparison by unpaired two-tailed Mann-Whitney U-tests (C) or two-way ANOVA with Bonferroni post hoc tests (D).

DISCUSSION

Here, we have demonstrated a protective role for the immune regulator IRAK-M in the metabolic

and immune homeostasis of the RPE. A feed-forward loop with aging, oxidative stress, and a decline in abundance of IRAK-M may generate a pro-inflammatory microenvironment driving retinal degeneration. We have shown that replenishing IRAK-M can maintain mitochondrial function, inhibit senescence, and promote cell survival, protecting the retina from degeneration in a LIRD mouse model and *Irak3*$^{-/-}$ mice. Because IRAK-M is reduced with aging, oxidative stress, and AMD, the replenishment of IRAK-M may be a therapeutic strategy for treating patients with AMD.

Previous research has demonstrated the expression of IRAK-M in cells other than monocytes/macrophages, including airway and intestine epithelium, fibroblasts, neurons, neutrophils, dendritic cells basophils, and B cells (*39*, *57*, *58*). Mutant *IRAK3* has been link to asthma (*32*). Tarallo *et al.* (*16*) reported aberrant activation of NLRP3-inflammasome and Myddosome signaling, such as increased phospho-IRAK1/4 expression in RPE lysates of patients with geographic atrophy, but did not probe IRAK-M. Here, we found that the abundance of IRAK-M declines with age in the RPE but not retinal tissue and is reduced further in patients with AMD compared to age-matched controls. Furthermore, IRAK-M was expressed by bilayer ciliary epithelium, suggesting distribution in other ocular epithelium barriers. The RPE regulates and protects against excessive oxidative stressors, inflammasome activation, mitochondrial impairment, lipid accumulation, and cellular senescence (*4*, *17*, *26*, *59*), all pathways that can accelerate AMD progression (*13*, *14*). We showed that *Irak3*$^{-/-}$ mice incurred greater oxidative damage, including RPE cell mitochondrial dysfunction, senescence, and early AMD-like pathologies such as subretinal accumulation of myeloid cells, outer retinal lesions, and cell death. The focal RPE cell death seen here in *Irak3*$^{-/-}$ mice supports findings of RPE heterogeneity in mice, like humans (*60–62*), and has been observed in other murine models of retinal degeneration, such as *Ccl2/ Cx3cr1* (CX3C motif chemokine receptor 1) double KO (DKO), *LysMCre-Socs3*$^{fl/fl}$*Cx3cr1*$^{gfp/gfp}$ DKO, and systemic injection of sodium iodate (*63–65*).

Differential expression of IRAK-M is context-dependent in different disease settings. For instance, up-regulation of IRAK-M was identified after ischemia-reperfusion of the liver and brain (*66*, *67*), and in the infarcted heart (*68*), where it was thought to limit the magnitude of immune responses and repair pro-inflammatory damage. In a mouse model of cerebral ischemia, IRAK-M was induced by hypoxia-inducible factor 1 subunit alpha and played a neuroprotective role by inhibition of NF-κB signaling and production of cyclooxygenase 2, TNF-α, NLRP3, and inducible nitric oxide synthase. In comparison, *Irak3*$^{-/-}$ mice developed exacerbated infarcts (*58*). In contrast to acute responses, down-regulation of IRAK-M expression was associated with chronic

diseases, exemplified by alcoholic liver disease, inflammatory bowel disease, insulin resistance, and metabolic syndrome (*25*, *30*, *31*). Although acute alcohol intake increases IRAK-M abundance in human monocytes, chronic alcohol exposure results in decreased abundance and enhanced inflammation (*69*). In patients with obesity, reduced *IRAK3* expression in monocytes and adipose tissues leads to mitochondrial oxidative stress and systemic inflammation (*31*). Furthermore, age-related decreases in the basal expression of IRAK-M and its inducibility upon TLR activation have been found in peripheral blood mononuclear cells and fibroblasts in rodents (*70*, *71*). We localized the decline in IRAK-M expression to the RPE, rather than to the retina or choroid, in aging, oxidative stress, and AMD, and increasing IRAK-M in the RPE via boosting endogenous gene expression or exogenous gene delivery helped to maintain mitochondrial activity and autophagy and inhibit cellular senescence and NF-κB activity, supporting the importance of IRAK-M for RPE health.

Several limitations exist in this study. First, the influence of rhythmic/circadian PR outer segment phagocytosis on IRAK-M abundance in the RPE remains unknown. Given the challenges in obtaining consecutive human postmortem RPE samples for circadian analysis, collecting murine RPE samples during daytime and nighttime intervals could offer insights into this investigation for expression and gene regulation. Second, we cannot rule out a potential contribution of IRAK-M from other cell types to outer retinal degeneration. Conditional KO mice via Cre/loxP or CRISPR-Cas9 will be essential for discerning pathologies arising from IRAK-M deficiency or inactivation in specific cell types, for example, the RPE or retinal microglia. Third, because of the restricted availability of human donor eyes, we could not pinpoint the specific stage of AMD at which IRAK-M abundance is predominantly affected. Fourth, our in vivo assessment did not show ocular toxicity when overexpressing IRAK-M for more than 6 months in *Irak3*$^{-/-}$ mice. However, note that all murine models of retinal degeneration, including the *Irak3*$^{-/-}$ mice and the murine LIRD model, do not exactly phenocopy human AMD (*72*); for preclinical safety and efficacy assessment, large animal studies will be required. Last, although early passages of the ARPE-19 cell line share RPE features, they are not fully differentiated RPE cells. Data from ARPE-19 cells should be used to supplement findings from human samples, in vivo and primary cell experiments.

In conclusion, we have identified an age-related decline of IRAK-M abundance, largely restricted to the RPE, which is worsened in AMD. Our findings suggest that IRAK-M plays a crucial role in maintaining RPE cell homeostasis and function via cotargeting mitochondrial health, oxidative stress, autophagy, and inflammation. Gene augmentation of IRAK-M demonstrates translational benefit in counteracting side effects of aging or oxidative stress and

reducing outer retinal degeneration in preclinical disease models, suggesting a therapeutic strategy via manipulating IRAK-M in the RPE in patients with AMD.

MATERIALS AND METHODS

Study design

The overall goals of this study were to define IRAK-M expression in RPE during the aging process and in AMD. The subsequent goal was to develop targeted gene therapy for age-related and inflammation-driven RPE and retinal degeneration. For investigations on human ocular samples in all respective institutions, experiments were conducted according to the Declaration of Helsinki principles and in compliance with approved institutional guidelines. All animal protocols were approved by the University of Bristol Ethical Review Group. The primary experimental procedures are described below, with detailed descriptions listed in Supplementary Materials and Methods.

For microarray analyses of age-related progressive changes in mRNA expression of IRAKs in human ocular samples, donor ages ranged from 35 to 97 years old (mostly between 65 and 85). Samples were collected from donors without clinically recorded AMD (color fundus and/or OCT imaging) where patient medical files could be queried. For donor eye tissue samples where no ocular history was available, we carefully analyzed the macular region of dissected globes under a dissecting microscope for drusen, RPE hyperpigmentation, and indications of CNV bleeding. Samples were processed and run on a microarray platform in a random nonsequential order. All samples were given a random sample number and blinded to all scientists. For age-dependent results, the sample identity was unknown, and only the microarray gene probe name, intensity, and age were compared. Inclusion required ocular tissue samples with no clinically recorded or obvious tissue AMD pathology and total mRNA RIN scores ≥7. Samples that had obvious AMD or RIN scores <7 were excluded from these analyses.

Age- or AMD-related changes of IRAK-M protein expression in human ocular tissues were determined by Western blot or IHC using postmortem eye tissues or paraffin-embedded sections, respectively. The absence of other comorbid ocular diseases or clinically classified AMD stage of individual donor eye samples was identified by eye banks (see the Supplementary Materials) according to the medical records. Sections from donor eyes diagnosed with wet AMD were excluded from the IHC study. All samples were randomly selected from each group for analysis.

For clinical assessment of retinal pathology in different murine models associated with aging, IRAK-M deficiency, or oxidative stress, eyes were examined at indicated time points using Micron

IV–guided fundoscopy and OCT and assessed by investigators blinded to the origin of images. For assessment of IRAK-M replenishment by subretinal administration of AAV2-expressing human *IRAK3* in mice, animals were randomly allocated to different treatment groups. The subretinal injection procedure created a temporary subretinal bleb, where a part of the retina was elevated and separated from the RPE to accommodate the injected fluid. Mice that had no retinal blebs immediately after the injection were excluded from the study. In all cases, null AAV2 vehicle injections served as a negative control to determine baseline tissue responses. The laterality of injected eyes was randomized, and the investigators were blinded to the vector type throughout intervention and analysis. The sample size was chosen empirically on the basis of the results of previous studies and preliminary experiments according to the 3R principles and varied between experimental settings. In animal experiments, we collected all samples during the daytime (lights ON between 7:00 a.m. and 7:00 p.m.) to avoid potential day-night fluctuation. For all experiments, the number of replicates, statistical tests used, and *P* values are reported in the figure legends.

Human sample analyses

We used a gene burden test on the GWAS data (*6*) to analyze whether there was a genetic association between rare variants of *IRAK3* and AMD, compared to other Myddosome-associated genes. Microarray analysis was used to explore age-related changes in mRNA expression of *IRAKs* in extramacular and macula RPE/choroid or retina. AMD-associated changes in mRNA expression of *IRAKs* and known genes involved in the negative regulation of TLR/IL-1R/MyD88/IRAK1/4 pathways were discerned by data mining of RNA-seq data (GSE99248). AMD-associated changes in IRAK-M protein expression were examined by IHC of postmortem eye sections from patients with AMD or age-matched controls. The processing and staining of all sections were executed at the same time with the same vials of reagents and antibodies to avoid batch effects.

Irak3$^{-/-}$, aging mice, and oxidative stress induction

We used *Irak3*$^{-/-}$ and WT mice to define whether aging and/or lack of *I*RAK-M affected outer retinal degeneration. Only male mice from the established *Rd8*-negative *Irak3*$^{-/-}$ colony were used to avoid possible sex-associated variation in immune responsiveness (*73*). Clinical examinations on retinal pathology, including retinal structure, fundus spots, and thickness, were performed using Micron IV–guided fundoscopy and OCT in *Irak3*$^{-/-}$ mice (aged 2 to 15 months) and WT mice (aged 2 to 21 months). Primary endpoints were RPE cell death, subretinal accumulation of macrophages, and cytokine expression at indicated time points. To determine whether oxidative stress could be an independent factor affecting IRAK-M expression, we applied

oxidative stressors to different RPE cells in vitro and 8-week-old WT mice in vivo. Two types of LIRD models with different severity of outer retinal injury were performed via fundus camera–directed light exposure using either a light-only protocol (100 kilolux for 20 min) or an FL-assisted light challenge protocol where overnight dark-adapted mice were intraperitoneally administered with 100 μl of 2% FL before light challenge to the retina (16 kilolux for 5 min) (*46*). Paraquat-induced retinal degeneration was conducted by intravitreal injection of paraquat diluted in phosphate-buffered saline (PBS) (2 μl; 1.5 mM) (*47*). The contralateral eye was left without light challenge or injected intravitreally with PBS as a control.

To elucidate metabolic mechanisms involved in *Irak3*-KO–induced retinal degeneration, we isolated primary RPE cells from 5-month-old *Irak3*$^{-/-}$ versus WT littermates and characterized cell metabolism and senescent phenotype. To demonstrate whether IRAK-M had a protecting role for RPE cells against oxidative or immune challenges in vitro, we overexpressed *IRAK3* by either endogenous CRISPR-Cas9 activation or exogenous *IRAK3* delivery via plasmid vectors. In vitro cell responses to stressors and *IRAK3* gene delivery were assessed for mitochondrial respiration and glycolytic activities, autophagy flux, cytokine secretion, and expression of senescence markers (see Supplementary Materials and Methods).

Therapeutic approaches

Subretinal administration of AAV2-expressing human *IRAK3* in two murine models of retinal degeneration, light-induced outer retinal degeneration in young WT mice and spontaneous outer retinal degeneration in aging *Irak3*$^{-/-}$ mice. In both models, null AAV2 vehicle injections served as a negative control to determine baseline responses. The control AAV2 and *IRAK3*-expressing AAV2 were both under the control of constitutive CMV- or RPE-specific Best1 promoter. A pilot experiment to determine viral dose-dependent transduction efficacy was performed by subretinal injection of 2×10^9 gc (high dose) or 4×10^8 gc (low dose) of AAV2.CMV.EGFP to each eye and evaluated by fundal fluorescence imaging for 11 weeks. AAV-mediated human *IRAK3* transgene expression in mice RPE/retina was verified by qRT-PCR and IHC of retinal samples. Retinas were exposed to light challenge at 2 (LIRD) or 3 (FL- LIRD) weeks after AAV injection, and retinal pathologies were examined 2 weeks after AAV injection by fundoscopy, OCT, and histology for TUNEL$^+$ cell death and mitochondrial content. *Irak3*$^{-/-}$ mice (2 to 4 months old) were monitored for 6 months after subretinal injection of AAV vectors using quantitative parameters such as retinal fundus spots and outer retinal thickness, measured by fundoscopy and OCT.

Statistical analysis

Results are presented as means ± SD. A simple linear regression was used using GraphPad Prism 9.5 to analyze the correlation between gene expression and human aging using microarray data. All other statistical analyses were conducted using Prism 10.1.2. All primary data associated with the statistical analyses are presented in data file S1. For data analysis on experiments with one variable, the normal distribution of samples was determined using the Shapiro-Wilk test, and equality in variances across groups with normal data was measured using the *F* test for two groups or Brown-Forsythe test for more than two groups (data file S2). Comparison between two groups with a single variable was performed using unpaired two-tailed Student's *t* test for normal data with equal variances, Welch's *t* test for normal data with unequal variances, or Mann-Whitney *U* test if at least one group has nonnormal samples. For experiments involving more than two groups and one variable, comparisons were measured using one-way analysis of variance (ANOVA) followed by Bonferroni post hoc multiple comparisons tests if all groups are normal and equal, Brown-Forsythe and Welch ANOVA with Dunnett's T3 tests if groups are normal but unequal, or Kruskal-Wallis ANOVA with Dunn's tests if at least one group is nonnormal. In experiments involving two independent variables, we used two-way ANOVA followed by Bonferroni post hoc tests for all human samples, in vitro, and most animal experiments. In experiments assessing the impact of acute oxidative stress (induced by light or intravitreal injection of paraquat) on murine retinal thickness (Fig. 4, C, F, and G), Holm-Sidak post hoc tests were used to enhance statistical power and minimize the need for additional animals in the experiments. For two-way ANOVA, certain degrees of nonnormally distributed data can be tolerated by ANOVA, which is robust to violations of normality (*74*, *75*). All specific statistical tests and post hoc methods are specified in figure legends. Differences between groups were considered significant at $P < 0.05$.

Supplementary Materials

This PDF file includes:

scitranslmed.adi4125_sm.pdf

Materials and Methods

Figs. S1 to S14

Tables S1 and S2

References (*76–82*)

Other Supplementary Material for this manuscript includes the following:

scitranslmed.adi4125_data_files_s1_and_s2.zip

Data files S1 and S2

scitranslmed.adi4125_mdar_reproducibility_checklist.pdf

MDAR Reproducibility Checklist

REFERENCES AND NOTES

1 J. Moretti, J. M. Blander, Cell-autonomous stress responses in innate immunity. J. Leukoc. Biol. 101, 77–86 (2017).

2 C. Franceschi, P. Garagnani, P. Parini, C. Giuliani, A. Santoro, Inflammaging: A new immune-metabolic viewpoint for age-related diseases. Nat. Rev. Endocrinol. 14, 576–590 (2018).

3 Y. Tong, S. Wang, Not all stressors are equal: Mechanism of stressors on RPE cell degeneration. Front. Cell Dev. Biol. 8, 591067 (2020).

4 D. A. Copland, S. Theodoropoulou, J. Liu, A. D. Dick, A perspective of AMD through the eyes of immunology. Invest. Ophthalmol. Vis. Sci. 59, AMD83–AMD92 (2018).

5 J. T. Handa, C. Bowes Rickman, A. D. Dick, M. B. Gorin, J. W. Miller, C. A. Toth, M. Ueffing, M. Zarbin, L. A. Farrer, A systems biology approach towards understanding and treating non-neovascular age-related macular degeneration. Nat. Commun. 10, 3347 (2019).

6 L. G. Fritsche, W. Igl, J. N. Bailey, F. Grassmann, S. Sengupta, J. L. Bragg-Gresham, K. P. Burdon, S. J. Hebbring, C. Wen, M. Gorski, I. K. Kim, D. Cho, D. Zack, E. Souied, H. P. Scholl, E. Bala, K. E. Lee, D. J. Hunter, R. J. Sardell, P. Mitchell, J. E. Merriam, V. Cipriani, J. D. Hoffman, T. Schick, Y. T. Lechanteur, R. H. Guymer, M. P. Johnson, Y.

Jiang, C. M. Stanton, G. H. Buitendijk, X. Zhan, A. M. Kwong, A. Boleda, M. Brooks, L. Gieser, R. Ratnapriya, K. E. Branham, J. R. Foerster, J. R. Heckenlively, M. I. Othman, B. J. Vote, H. H. Liang, E. Souzeau, I. L. McAllister, T. Isaacs, J. Hall, S. Lake, D. A. Mackey, I. J. Constable, J. E. Craig, T. E. Kitchner, Z. Yang, Z. Su, H. Luo, D. Chen, H. Ouyang, K. Flagg, D. Lin, G. Mao, H. Ferreyra, K. Stark, C. N. von Strachwitz, A. Wolf, C. Brandl, G. Rudolph, M. Olden, M. A. Morrison, D. J. Morgan, M. Schu, J. Ahn, G. Silvestri, E. E. Tsironi, K. H. Park, L. A. Farrer, A. Orlin, A. Brucker, M. Li, C. A. Curcio, S. Mohand-Saïd, J. A. Sahel, I. Audo, M. Benchaboune, A. J. Cree, C. A. Rennie, S. V. Goverdhan, M. Grunin, S. Hagbi-Levi, P. Campochiaro, N. Katsanis, F. G. Holz, F. Blond, H. Blanché, J. F. Deleuze, R. P. Igo, B. Truitt, N. S. Peachey, S. M. Meuer, C. E. Myers, E. L. Moore, R. Klein, M. A. Hauser, E. A. Postel, M. D. Courtenay, S. G. Schwartz, J. L. Kovach, W. K. Scott, G. Liew, A. G. Tan, B. Gopinath, J. C. Merriam, R. T. Smith, J. C. Khan, H. Shahid, A. T. Moore, J. A. McGrath, R. Laux, M. A. Brantley, A. Agarwal, L. Ersoy, A. Caramoy, T. Langmann, N. T. Saksens, E. K. de Jong, C. B. Hoyng, M. S. Cain, A. J. Richardson, T. M. Martin, J. Blangero, D. E. Weeks, B. Dhillon, C. M. van Duijn, K. F. Doheny, J. Romm, C. C. Klaver, C. Hayward, M. B. Gorin, M. L. Klein, P. N. Baird, A. I. den Hollander, S. Fauser, J. R. Yates, R. Allikmets, J. J. Wang, D. A. Schaumberg, B. E. Klein, S. A. Hagstrom, I. Chowers, A. J. Lotery, T. Léveillard, K. Zhang, M. H. Brilliant, A. W. Hewitt, A. Swaroop, E. Y. Chew, M. A. Pericak-Vance, M. DeAngelis, D. Stambolian, J. L. Haines, S. K. Iyengar, B. H. Weber, G. R. Abecasis, I. M. Heid, A large genome-wide association study of age-related macular degeneration highlights contributions of rare and common variants. Nat. Genet. 48, 134–143 (2016).

7 T. W. Winkler, F. Grassmann, C. Brandl, C. Kiel, F. Günther, T. Strunz, L. Weidner, M. E. Zimmermann, C. A. Korb, A. Poplawski, A. K. Schuster, M. Müller-Nurasyid, A. Peters, F. G. Rauscher, T. Elze, K. Horn, M. Scholz, M. Cañadas-Garre, A. J. McKnight, N. Quinn, R. E. Hogg, H. Küchenhoff, I. M. Heid, K. J. Stark, B. H. F. Weber, Genome-wide association meta-analysis for early age-related macular degeneration highlights novel loci and insights for advanced disease. BMC Med. Genomics 13, 120 (2020).

8 H. Khan, A. A. Aziz, H. Sulahria, A. Ahmed, N. Choudhry, R. Narayanan, C. Danzig, A. M. Khanani, Emerging treatment options for geographic atrophy (GA) secondary to age-related macular degeneration. Clin. Ophthalmol. 17, 321–327 (2023).

9 B. L. Yaspan, D. F. Williams, F. G. Holz, C. D. Regillo, Z. Li, A. Dressen, M. van Lookeren Campagne, K. N. Le, R. R. Graham, T. Beres, T. R. Bhangale, L. A. Honigberg, A. Smith, E. C. Henry, C. Ho, E. C. Strauss, M. S. Investigators, Targeting

factor D of the alternative complement pathway reduces geographic atrophy progression secondary to age-related macular degeneration. Sci. Transl. Med. 9, eaaf1443 (2017).

10 B. Calippe, S. Augustin, F. Beguier, H. Charles-Messance, L. Poupel, J. B. Conart, S. J. Hu, S. Lavalette, A. Fauvet, J. Rayes, O. Levy, W. Raoul, C. Fitting, T. Denèfle, M. C. Pickering, C. Harris, S. Jorieux, P. M. Sullivan, J. A. Sahel, P. Karoyan, P. Sapieha, X. Guillonneau, E. L. Gautier, F. Sennlaub, Complement factor H inhibits CD47-mediated resolution of inflammation. Immunity 46, 261–272 (2017).

11 F. Beguier, M. Housset, C. Roubeix, S. Augustin, Y. Zagar, C. Nous, T. Mathis, C. Eandi, M. Benchaboune, A. Drame-Maigné, W. Carpentier, S. Chardonnet, S. Touhami, G. Blot, J. B. Conart, H. Charles-Messance, A. Potey, J. F. Girmens, M. Paques, F. Blond, T. Leveillard, E. Koertvely, J. E. Roger, J. A. Sahel, P. Sapieha, C. Delarasse, X. Guillonneau, F. Sennlaub, The 10q26 risk haplotype of age-related macular degeneration aggravates subretinal inflammation by impairing monocyte elimination. Immunity 53, 429–441.e8 (2020).

12 C. B. Toomey, U. Kelly, D. R. Saban, C. Bowes Rickman, Regulation of age-related macular degeneration-like pathology by complement factor H. Proc. Natl. Acad. Sci. U.S.A. 112, E3040–E3049 (2015).

13 S. Romero-Vazquez, V. Llorens, A. Soler-Boronat, M. Figueras-Roca, A. Adan, B. Molins, Interlink between inflammation and oxidative stress in age-related macular degeneration: Role of complement factor H. Biomedicine 9, 763 (2021).

14 W. A. Tseng, T. Thein, K. Kinnunen, K. Lashkari, M. S. Gregory, P. A. D'Amore, B. R. Ksander, NLRP3 inflammasome activation in retinal pigment epithelial cells by lysosomal destabilization: Implications for age-related macular degeneration. Invest. Ophthalmol. Vis. Sci. 54, 110–120 (2013).

15 A. Klettner, J. Roider, Retinal pigment epithelium expressed Toll-like receptors and their potential role in age-related macular degeneration. Int. J. Mol. Sci. 22, 8387 (2021).

16 V. Tarallo, Y. Hirano, B. D. Gelfand, S. Dridi, N. Kerur, Y. Kim, W. G. Cho, H. Kaneko, B. J. Fowler, S. Bogdanovich, R. J. Albuquerque, W. W. Hauswirth, V. A. Chiodo, J. F. Kugel, J. A. Goodrich, S. L. Ponicsan, G. Chaudhuri, M. P. Murphy, J. L. Dunaief, B. K. Ambati, Y. Ogura, J. W. Yoo, D. K. Lee, P. Provost, D. R. Hinton, G. Núñez, J. Z. Baffi, M. E. Kleinman, J. Ambati, DICER1 loss and Alu RNA induce age-related macular degeneration via the NLRP3 inflammasome and MyD88. Cell 149, 847–859 (2012).

17 K. S. Lee, S. Lin, D. A. Copland, A. D. Dick, J. Liu, Cellular senescence in the aging retina and developments of senotherapies for age-related macular degeneration. J.

Neuroinflammation 18, 32 (2021).

18 K. Mulfaul, M. Rhatigan, S. Doyle, Toll-like receptors and age-related macular degeneration. Adv. Exp. Med. Biol. 1074, 19–28 (2018).

19 L. Ma, F. Y. Tang, W. K. Chu, A. L. Young, M. E. Brelen, C. P. Pang, L. J. Chen, Association of Toll-like receptor 3 polymorphism rs3775291 with age-related macular degeneration: A systematic review and meta-analysis. Sci. Rep. 6, 19718 (2016).

20 M. Hata, E. M. M. A. Andriessen, R. Diaz-Marin, F. Fournier, S. Crespo-Garcia, G. Blot, R. Juneau, F. Pilon, A. Dejda, V. Guber, E. Heckel, C. Daneault, V. Calderon, C. Des Rosiers, H. J. Melichar, T. Langmann, J. S. Joyal, A. M. Wilson, P. Sapieha, Past history of obesity triggers persistent epigenetic changes in innate immunity and exacerbates neuroinflammation. Science 379, 45–62 (2023).

21 M. Kader, M. Alaoui-El-Azher, J. Vorhauer, B. B. Kode, J. Z. Wells, D. Stolz, G. Michalopoulos, A. Wells, M. Scott, N. Ismail, MyD88-dependent inflammasome activation and autophagy inhibition contributes to Ehrlichia-induced liver injury and toxic shock. PLOS Pathog. 13, e1006644 (2017).

22 S. Wang, Y. Zheng, Q. Li, X. He, R. Ren, W. Zhang, M. Song, H. Hu, F. Liu, G. Sun, S. Sun, Z. Liu, Y. Yu, P. Chan, G. G. Zhao, Q. Zhou, G. H. Liu, F. Tang, J. Qu, Deciphering primate retinal aging at single-cell resolution. Protein Cell 12, 889–898 (2021).

23 J. Liu, D. A. Copland, S. Theodoropoulou, H. A. Chiu, M. D. Barba, K. W. Mak, M. Mack, L. B. Nicholson, A. D. Dick, Impairing autophagy in retinal pigment epithelium leads to inflammasome activation and enhanced macrophage-mediated angiogenesis. Sci. Rep. 6, 20639 (2016).

24 A. J. Clare, J. Liu, D. A. Copland, S. Theodoropoulou, A. D. Dick, Unravelling the therapeutic potential of IL-33 for atrophic AMD. Eye (Lond.) 36, 266–272 (2022).

25 A. Jain, S. Kaczanowska, E. Davila, IL-1 receptor-associated kinase signaling and its role in inflammation, cancer progression, and therapy resistance. Front. Immunol. 5, 553 (2014).

26 R. Gill, A. Tsung, T. Billiar, Linking oxidative stress to inflammation: Toll-like receptors. Free Radic. Biol. Med. 48, 1121–1132 (2010).

27 J. Du, G. A. Nicolaes, D. Kruijswijk, M. Versloot, T. van der Poll, C. van't Veer, The structure function of the death domain of human IRAK-M. Cell Commun. Signal 12, 77 (2014).

28 H. Zhou, M. Yu, K. Fukuda, J. Im, P. Yao, W. Cui, K. Bulek, J. Zepp, Y. Wan, T. W. Kim, W. Yin, V. Ma, J. Thomas, J. Gu, J. A. Wang, P. E. DiCorleto, P. L. Fox, J. Qin, X. Li,

IRAK-M mediates Toll-like receptor/IL-1R-induced NFκB activation and cytokine production. EMBO J. 32, 583–596 (2013).

29 K. Lyroni, A. Patsalos, M. G. Daskalaki, C. Doxaki, B. Soennichsen, M. Helms, I. Liapis, V. Zacharioudaki, S. C. Kampranis, C. Tsatsanis, Epigenetic and transcriptional regulation of IRAK-M expression in macrophages. J. Immunol. 198, 1297–1307 (2017).

30 L. L. Hubbard, B. B. Moore, IRAK-M regulation and function in host defense and immune homeostasis. Infect. Dis. Rep. 2, e9 (2010).

31 M. Hulsmans, B. Geeraert, D. De Keyzer, A. Mertens, M. Lannoo, B. Vanaudenaerde, M. Hoylaerts, N. Benhabiles, C. Tsatsanis, C. Mathieu, P. Holvoet, Interleukin-1 receptor-associated kinase-3 is a key inhibitor of inflammation in obesity and metabolic syndrome. PLOS ONE 7, e30414 (2012).

32 L. Balaci, M. C. Spada, N. Olla, G. Sole, L. Loddo, F. Anedda, S. Naitza, M. A. Zuncheddu, A. Maschio, D. Altea, M. Uda, S. Pilia, S. Sanna, M. Masala, L. Crisponi, M. Fattori, M. Devoto, S. Doratiotto, S. Rassu, S. Mereu, E. Giua, N. G. Cadeddu, R. Atzeni, U. Pelosi, A. Corrias, R. Perra, P. L. Torrazza, P. Pirina, F. Ginesu, S. Marcias, M. G. Schintu, G. S. Del Giacco, P. E. Manconi, G. Malerba, A. Bisognin, E. Trabetti, A. Boner, L. Pescollderungg, P. F. Pignatti, D. Schlessinger, A. Cao, G. Pilia, IRAK-M is involved in the pathogenesis of early-onset persistent asthma. Am. J. Hum. Genet. 80, 1103–1114 (2007).

33 L. M. Scott, E. E. Vincent, N. Hudson, C. Neal, N. Jones, E. C. Lavelle, M. Campbell, A. P. Halestrap, A. D. Dick, S. Theodoropoulou, Interleukin-33 regulates metabolic reprogramming of the retinal pigment epithelium in response to immune stressors. JCI Insight 6, e129429 (2021).

34 H. Xi, K. J. Katschke, Y. Li, T. Truong, W. P. Lee, L. Diehl, L. Rangell, J. Tao, R. Arceo, J. Eastham-Anderson, J. A. Hackney, A. Iglesias, J. Cote-Sierra, J. Elstrott, R. M. Weimer, M. van Lookeren Campagne, IL-33 amplifies an innate immune response in the degenerating retina. J. Exp. Med. 213, 189–207 (2016).

35 J. Augustine, S. Pavlou, I. Ali, K. Harkin, E. Ozaki, M. Campbell, A. W. Stitt, H. Xu, M. Chen, IL-33 deficiency causes persistent inflammation and severe neurodegeneration in retinal detachment. J. Neuroinflammation 16, 251 (2019).

36 E. J. Kim, G. R. Grant, A. S. Bowman, N. Haider, H. V. Gudiseva, V. R. M. Chavali, Complete transcriptome profiling of normal and age-related macular degeneration eye tissues reveals dysregulation of anti-sense transcription. Sci. Rep. 8, 3040 (2018).

37 J. Tode, E. Richert, S. Koinzer, A. Klettner, C. von der Burchard, R. Brinkmann, R.

Lucius, J. Roider, Selective retina therapy reduces bruch's membrane thickness and retinal pigment epithelium pathology in age-related macular degeneration mouse models. Transl. Vis. Sci. Technol. 8, 11 (2019).

38 D. E. Rothschild, Y. Zhang, N. Diao, C. K. Lee, K. Chen, C. C. Caswell, D. J. Slade, R. F. Helm, T. LeRoith, L. Li, I. C. Allen, Enhanced mucosal defense and reduced tumor burden in mice with the compromised negative regulator IRAK-M. EBioMedicine 15, 36–47 (2017).

39 K. Kobayashi, L. D. Hernandez, J. E. Galán, C. A. Janeway, R. Medzhitov, R. A. Flavell, IRAK-M is a negative regulator of Toll-like receptor signaling. Cell 110, 191–202 (2002).

40 S. M. Lange, M. I. Nelen, P. Cohen, Y. Kulathu, Dimeric structure of the pseudokinase IRAK3 suggests an allosteric mechanism for negative regulation. Structure 29, 238–251 (2021).

41 P. Herrmann, J. A. Cowing, E. Cristante, S. E. Liyanage, J. Ribeiro, Y. Duran, L. Abelleira Hervas, L. S. Carvalho, J. W. Bainbridge, U. F. Luhmann, R. R. Ali, Cd59a deficiency in mice leads to preferential innate immune activation in the retinal pigment epithelium-choroid with age. Neurobiol. Aging 36, 2637–2648 (2015).

42 N. K. Wang, H. F. Fine, S. Chang, C. L. Chou, W. Cella, J. Tosi, C. S. Lin, T. Nagasaki, S. H. Tsang, Cellular origin of fundus autofluorescence in patients and mice with a defective NR2E3 gene. Br. J. Ophthalmol. 93, 1234–1240 (2009).

43 N. L. Hawes, B. Chang, G. S. Hageman, S. Nusinowitz, P. M. Nishina, B. S. Schneider, R. S. Smith, T. H. Roderick, M. T. Davisson, J. R. Heckenlively, Retinal degeneration 6 (rd6): A new mouse model for human retinitis punctata albescens. Invest. Ophthalmol. Vis. Sci. 41, 3149–3157 (2000).

44 G. Venturini, D. Kokona, B. L. Steiner, E. G. Bulla, J. Jovanovic, M. S. Zinkernagel, P. Escher, In vivo analysis of onset and progression of retinal degeneration in the Nr2e3rd7/rd7 mouse model of enhanced S-cone sensitivity syndrome. Sci. Rep. 11, 19032 (2021).

45 K. Makabe, S. Sugita, M. Mandai, Y. Futatsugi, M. Takahashi, Microglia dynamics in retinitis pigmentosa model: Formation of fundus whitening and autofluorescence as an indicator of activity of retinal degeneration. Sci. Rep. 10, 14700 (2020).

46 Y. Ding, B. Aredo, X. Zhong, C. X. Zhao, R. L. Ufret-Vincenty, Increased susceptibility to fundus camera-delivered light-induced retinal degeneration in mice deficient in oxidative stress response proteins. Exp. Eye Res. 159, 58–68 (2017).

47 C. Cingolani, B. Rogers, L. Lu, S. Kachi, J. Shen, P. A. Campochiaro, Retinal degeneration from oxidative damage. Free Radic. Biol. Med. 40, 660–669 (2006).

48 P. Jin, L. Bo, Y. Liu, W. Lu, S. Lin, J. Bian, X. Deng, Activator protein 1 promotes the transcriptional activation of IRAK-M. Biomed. Pharmacother. 83, 1212–1219 (2016).

49 M. A. Kanow, M. M. Giarmarco, C. S. Jankowski, K. Tsantilas, A. L. Engel, J. Du, J. D. Linton, C. C. Farnsworth, S. R. Sloat, A. Rountree, I. R. Sweet, K. J. Lindsay, E. D. Parker, S. E. Brockerhoff, M. Sadilek, J. R. Chao, J. B. Hurley, Biochemical adaptations of the retina and retinal pigment epithelium support a metabolic ecosystem in the vertebrate eye. eLife 6, e28899 (2017).

50 S. Russell, J. Bennett, J. A. Wellman, D. C. Chung, Z. F. Yu, A. Tillman, J. Wittes, J. Pappas, O. Elci, S. McCague, D. Cross, K. A. Marshall, J. Walshire, T. L. Kehoe, H. Reichert, M. Davis, L. Raffini, L. A. George, F. P. Hudson, L. Dingfield, X. Zhu, J. A. Haller, E. H. Sohn, V. B. Mahajan, W. Pfeifer, M. Weckmann, C. Johnson, D. Gewaily, A. Drack, E. Stone, K. Wachtel, F. Simonelli, B. P. Leroy, J. F. Wright, K. A. High, A. M. Maguire, Efficacy and safety of voretigene neparvovec (AAV2-hRPE65v2) in patients with RPE65-mediated inherited retinal dystrophy: A randomised, controlled, open-label, phase 3 trial. Lancet 390, 849–860 (2017).

51 L. H. Vandenberghe, P. Bell, A. M. Maguire, C. N. Cearley, R. Xiao, R. Calcedo, L. Wang, M. J. Castle, A. C. Maguire, R. Grant, J. H. Wolfe, J. M. Wilson, J. Bennett, Dosage thresholds for AAV2 and AAV8 photoreceptor gene therapy in monkey. Sci. Transl. Med. 3, 88ra54 (2011).

52 S. Koponen, E. Kokki, T. Tamminen, S. Ylä-Herttuala, AAV2 and AAV9 tropism and transgene expression in the mouse eye and major tissues after intravitreal and subretinal delivery. Front. Drug Deliv. 3, 795 (2023).

53 Y. B. Johari, A. C. Mercer, Y. Liu, A. J. Brown, D. C. James, Design of synthetic promoters for controlled expression of therapeutic genes in retinal pigment epithelial cells. Biotechnol. Bioeng. 118, 2001–2015 (2021).

54 D. M. Wu, X. Ji, M. V. Ivanchenko, M. Chung, M. Piper, P. Rana, S. K. Wang, Y. Xue, E. West, S. R. Zhao, H. Xu, M. Cicconet, W. Xiong, C. L. Cepko, Nrf2 overexpression rescues the RPE in mouse models of retinitis pigmentosa. JCI Insight 6, e145029 (2021).

55 J. J. Hunter, J. I. Morgan, W. H. Merigan, D. H. Sliney, J. R. Sparrow, D. R. Williams, The susceptibility of the retina to photochemical damage from visible light. Prog. Retin. Eye Res. 31, 28–42 (2012).

56 K. Yokoo, Y. Yamamoto, T. Suzuki, Ammonia impairs tight junction barriers by inducing mitochondrial dysfunction in Caco-2 cells. FASEB J. 35, e21854 (2021).

57 M. Zhang, W. Chen, W. Zhou, Y. Bai, J. Gao, Critical role of IRAK-M in regulating

antigen-induced airway inflammation. Am. J. Respir. Cell Mol. Biol. 57, 547–559 (2017).

58 Y. Ma, R. L. Haynes, R. L. Sidman, T. Vartanian, TLR8: An innate immune receptor in brain, neurons and axons. Cell Cycle 6, 2859–2868 (2007).

59 K. Kaarniranta, H. Uusitalo, J. Blasiak, S. Felszeghy, R. Kannan, A. Kauppinen, A. Salminen, D. Sinha, D. Ferrington, Mechanisms of mitochondrial dysfunction and their impact on age-related macular degeneration. Prog. Retin. Eye Res. 79, 100858 (2020).

60 D. Ortolan, R. Sharma, A. Volkov, A. Maminishkis, N. A. Hotaling, L. A. Huryn, C. Cukras, S. Di Marco, S. Bisti, K. Bharti, Single-cell-resolution map of human retinal pigment epithelium helps discover subpopulations with differential disease sensitivity. Proc. Natl. Acad. Sci. U.S.A. 119, e2117553119 (2022).

61 H. Lee, H. Y. Lee, J. B. Chae, C. W. Park, C. Kim, J. H. Ryu, J. Jang, N. Kim, H. Chung, Single-cell transcriptome of the mouse retinal pigment epithelium in response to a low-dose of doxorubicin. Commun. Biol. 5, 722 (2022).

62 S. Datta, M. Cano, G. Satyanarayana, T. Liu, L. Wang, J. Wang, J. Cheng, K. Itoh, A. Sharma, I. Bhutto, R. Kannan, J. Qian, D. Sinha, J. T. Handa, Mitophagy initiates retrograde mitochondrial-nuclear signaling to guide retinal pigment cell heterogeneity. Autophagy 19, 966–983 (2023).

63 X. Du, E. M. Byrne, M. Chen, H. Xu, Minocycline inhibits microglial activation and improves visual function in a chronic model of age-related retinal degeneration. Biomedicine 10, 3222 (2022).

64 J. Tuo, C. M. Bojanowski, M. Zhou, D. Shen, R. J. Ross, K. I. Rosenberg, D. J. Cameron, C. Yin, J. A. Kowalak, Z. Zhuang, K. Zhang, C. C. Chan, Murine ccl2/cx3cr1 deficiency results in retinal lesions mimicking human age-related macular degeneration. Invest. Ophthalmol. Vis. Sci. 48, 3827–3836 (2007).

65 A. Enzbrenner, R. Zulliger, J. Biber, A. M. Q. Pousa, N. Schäfer, C. Stucki, N. Giroud, M. Berrera, E. Kortvely, R. Schmucki, L. Badi, A. Grosche, D. Pauly, V. Enzmann, Sodium iodate-induced degeneration results in local complement changes and inflammatory processes in murine retina. Int. J. Mol. Sci. 22, 9218 (2021).

66 W. Li, R. Huang, X. Gong, Z. Zhao, L. Zhang, Q. Zhou, X. Jiang, H. Tie, J. Wan, B. Wang, Allicin attenuated hepatic ischemia/reperfusion injury in mice by regulating PPARγ-IRAK-M-TLR4 signal pathway. Food Funct. 13, 7361–7376 (2022).

67 C. Lyu, Y. Zhang, M. Gu, Y. Huang, G. Liu, C. Wang, M. Li, S. Chen, S. Pan, Y. Gu, IRAK-M deficiency exacerbates ischemic neurovascular injuries in experimental stroke mice. Front. Cell. Neurosci. 12, 504 (2018).

68 A. Saxena, A. V. Shinde, Z. Haque, Y. J. Wu, W. Chen, Y. Su, N. G. Frangogiannis, The role of interleukin receptor associated kinase (IRAK)-M in regulation of myofibroblast phenotype in vitro, and in an experimental model of non-reperfused myocardial infarction. J. Mol. Cell. Cardiol. 89, 223–231 (2015).

69 P. Mandrekar, S. Bala, D. Catalano, K. Kodys, G. Szabo, The opposite effects of acute and chronic alcohol on lipopolysaccharide-induced inflammation are linked to IRAK-M in human monocytes. J. Immunol. 183, 1320–1327 (2009).

70 Y. Li, E. A. Howell, A. S. Lagoo, M. Kuchibhatla, H. Pan, H. J. Cohen, S. A. Lagoo, Differential gene expression of interleukin-1 receptor associated kinase-1 and interleukin-1 receptor associated kinase-M in peripheral blood mononuclear cells of young and aged rats following preconditioning with endotoxin. Shock 31, 55–63 (2009).

71 H. Domon, K. Tabeta, T. Nakajima, K. Yamazaki, Age-related alterations in gene expression of gingival fibroblasts stimulated with Porphyromonas gingivalis. J. Periodontal Res. 49, 536–543 (2014).

72 M. E. Pennesi, M. Neuringer, R. J. Courtney, Animal models of age related macular degeneration. Mol. Aspects Med. 33, 487–509 (2012).

73 S. L. Klein, K. L. Flanagan, Sex differences in immune responses. Nat. Rev. Immunol. 16, 626–638 (2016).

74 M. E. Harrigan, A. R. Filous, C. P. Vadala, A. Webb, M. Pietrzak, Z. Sahenk, H. Prüss, P. J. Reiser, P. G. Popovich, W. D. Arnold, J. M. Schwab, Lesion level-dependent systemic muscle wasting after spinal cord injury is mediated by glucocorticoid signaling in mice. Sci. Transl. Med. 15, eadh2156 (2023).

75 M. J. Blanca, R. Alarcón, J. Arnau, R. Bono, R. Bendayan, Non-normal data: Is ANOVA still a valid option? Psicothema 29, 552–557 (2017).

76 A. L. Price, G. V. Kryukov, P. I. de Bakker, S. M. Purcell, J. Staples, L. J. Wei, S. R. Sunyaev, Pooled association tests for rare variants in exon-resequencing studies. Am. J. Hum. Genet. 86, 832–838 (2010).

77 B. Chang, R. Hurd, J. Wang, P. Nishina, Survey of common eye diseases in laboratory mouse strains. Invest. Ophthalmol. Vis. Sci. 54, 4974–4981 (2013).

78 R. Fernandez-Godino, D. L. Garland, E. A. Pierce, Isolation, culture and characterization of primary mouse RPE cells. Nat. Protoc. 11, 1206–1218 (2016).

79 M. C. Marazita, A. Dugour, M. D. Marquioni-Ramella, J. M. Figueroa, A. M. Suburo, Oxidative stress-induced premature senescence dysregulates VEGF and CFH expression in retinal pigment epithelial cells: Implications for age-related macular degeneration.

Redox Biol. 7, 78–87 (2016).

80 B. J. Raveney, D. A. Copland, A. D. Dick, L. B. Nicholson, TNFR1-dependent regulation of myeloid cell function in experimental autoimmune uveoretinitis. J. Immunol. 183, 2321–2329 (2009).

81 J. Liu, D. A. Copland, S. Horie, W. K. Wu, M. Chen, Y. Xu, B. Paul Morgan, M. Mack, H. Xu, L. B. Nicholson, A. D. Dick, Myeloid cells expressing VEGF and arginase-1 following uptake of damaged retinal pigment epithelium suggests potential mechanism that drives the onset of choroidal angiogenesis in mice. PLOS ONE 8, e72935 (2013).

82 H. Lee, R. Purohit, A. Patel, E. Papageorgiou, V. Sheth, G. Maconachie, A. Pilat, R. J. McLean, F. A. Proudlock, I. Gottlob, In vivo foveal development using optical coherence tomography. Invest. Ophthalmol. Vis. Sci. 56, 4537–4545 (2015).

Acknowledgments

We thank M. C. McIntyre, J. T. Handa, and B. C. Mansfield for helpful discussion and critical comments on the manuscript.

Funding: This work was funded by grants from Rosetrees Trust and Stoneygate Trust (Joint grant M418-F1 to ADD, to J.L. and D.A.C.), Underwood Trust (to A.D.D.), Macular Society (to A.D.D., J.L., and D.A.C.), and Sight Research UK (grant SAC052, to J.L., A.D.D., and D.A.C.). The work was also supported by an unrestricted grant to the Moran Eye Center from Research to Prevent Blindness Inc. and unrestricted funds from the Sharon Eccles Steele Center for Translation Medicine (to G.S.H.). We thank the IAMDGC, supported by the National Eye Institute of the NIH (grant 5R01EY022310). The work of I.M.H. was supported by the NIH (grants RES516564 and RES511967).

Author contributions: Conceptualization: A.D.D., J.L., Y.K.C., and L.B.N. Methodology: J.L., A.D.D., Y.K.C., G.S.H., I.M.H., M.G., B.T.R., U.G., M.J.R., E.L.F., R.G., P.J.C., D.A.C., and L.B.N. Investigation: J.L., Y.K.C., D.A.C., A.J.C., M.G., B.T.R., G.S.H., L.S., S.T., U.G., K.C., G.S., O.H.B., K.O., J.L.B.P., J.W., L.M.R., and Y.L. Visualization: A.D.D., J.L., Y.K.C., and L.B.N. Supervision: A.D.D., J.L., and Y.K.C. Writing—original draft: J.L., A.D.D., and Y.K.C. Writing—review a editing: All authors.

Competing interests: A.D.D., J.L., and Y.K.C. are named inventors on an international patent application no. PCT/EP2022/082518. A.D.D. and Y.K.C. are cofounders of Cirrus Therapeutics

and hold equity. J.L. and D.A.C. hold equity in Cirrus Therapeutics. A.D.D. is a consultant for Hubble Tx, Affibody, 4 DMT, Novartis, Roche, UCB, Amilera, Janssen, ActivBio, and Apellis. Y.K.C. is a consultant or an advisor to Ally Therapeutics, AlphaSights, Anjarium Biosciences, Arthur D. Little, Celestial Therapeutics, Cirrus Therapeutics, FirstThought, Pacira Biosciences, Santé, University of Bristol, and Xora Innovation and has received consulting fees and/or equity. R.G. is consultant for Roche, Genentech, Apellis, Novartis, and Bayer. The other authors declare that they have no competing interests.

Data and materials availability: All data associated with this study are present in the paper or the Supplementary Materials. Genetic data analyzed for gene burden tests (Table 1 and table S1) are accessible from the original paper (*6*) and permitted for sharing by respective Institutional Review Boards, and summary statistics reported in the paper are archived in the database of Genotypes and Phenotypes (dbGaP) under accession no. phs001039.v1.p1. Microarray data used to analyze the *IRAK3*, *IRAK1*, and *IRAK4* expression correlated with aging (Fig. 1C and fig. S2) are available from G.S.H. under a material transfer agreement with the University of Utah Technology Licensing Office.